

Washington University in St. Louis
Washington University Open Scholarship

Engineering and Applied Science Theses &
Dissertations

McKelvey School of Engineering

Spring 5-17-2019

Numerical Simulation of Flow Past NACA 0012 Airfoil Using a Co-Flow Jet at Different Injection Angles to Control Lift and Drag

Da Xiao

Washington University in St. Louis

Follow this and additional works at: https://openscholarship.wustl.edu/eng_etds



Part of the [Engineering Commons](#)

Recommended Citation

Xiao, Da, "Numerical Simulation of Flow Past NACA 0012 Airfoil Using a Co-Flow Jet at Different Injection Angles to Control Lift and Drag" (2019). *Engineering and Applied Science Theses & Dissertations*. 428.
https://openscholarship.wustl.edu/eng_etds/428

This Thesis is brought to you for free and open access by the McKelvey School of Engineering at Washington University Open Scholarship. It has been accepted for inclusion in Engineering and Applied Science Theses & Dissertations by an authorized administrator of Washington University Open Scholarship. For more information, please contact digital@wumail.wustl.edu.

WASHINGTON UNIVERSITY IN ST. LOUIS

James Mckelvey School of Engineering
Department of Mechanical Engineering and Material Science

Thesis Examination Committee:

Ramesh Agarwal, Chair

David Peters

Swami Karunamoorthy

Numerical Simulation of Flow Past NACA 0012 Airfoil Using a Co-Flow Jet at Different
Injection Angles to Control Lift and Drag

by

Da Xiao

A dissertation presented to the James Mckelvey School of Engineering
of Washington University in St. Louis
in partial fulfillment of the requirements for the degree of
Master of Science

May 2019
St. Louis, Missouri

Table of Contents

Table of Contents	ii
List of Figures	iii
List of Tables	v
Nomenclature	vi
Acknowledgments	viii
ABSTRACT OF THE THESIS	x
Chapter 1: Introduction	1
Chapter 2: CFJ Parameters	4
2.1 Lift and Drag Calculation	4
2.2 Jet Momentum Coefficient	6
Chapter 3: Physical Model and Mesh	7
3.1 Flow Conditions	7
3.2 Geometry and Mesh	7
3.3 V_j with Different Injection Angles	9
Chapter 4: Numerical Method	11
4.1 ANSYS FLUENT Setup and Boundary Conditions	11
4.2 UDF of C_μ Iteration	12
Chapter 5: Validation of Numerical Method	13
Chapter 6: Results and Discussion	15
6.1 Changeable injection angle's influence on aerodynamic coefficients	15
6.2 Sharp change in aerodynamic coefficient for a combination of C_μ , injection slot location and high injection angle	28
6.3 Injection angle's influence on stall angle	34
Chapter 7: Conclusions	41
References	43
Appendix	45
Curriculum Vita	66

List of Figures

Figure 1: CFJ and baseline airfoil.....	2
Figure 2: CFJ and FC airfoil.....	2
Figure 3: Flow parameters at the injection and suction slots.....	5
Figure 4: Computational domain and structured mesh.....	8
Figure 5: Refinement of the mesh near the changeable injection angle for CFJ NACA0012 airfoil.....	8
Figure 6: Changeable injection angle on the upper surface of the airfoil.....	9
Figure 7: Diagrammatic sketch describing how to calculate V_j	10
Figure 8: Pressure coefficient for flows past NACA0012 airfoil; $Re = 6 \times 10^6$, $\alpha = 10^\circ$	13
Figure 9: Streamlines and velocity vectors for flow past NACA0012 airfoil; $Re = 6 \times 10^6$, $\alpha = 10^\circ$	14
Figure 10: Lift coefficients variation with injection angle; $C\mu = 0.3$, $\alpha = 0^\circ$	16
Figure 11: Absolute changes in lift coefficients with injection angle; $C\mu = 0.3$, $\alpha = 0^\circ$	17
Figure 12: Relative changes in lift coefficients with injection angle; $C\mu = 0.3$, $\alpha = 0^\circ$	17
Figure 13: Drag coefficients variation with injection angle; $C\mu = 0.3$, $\alpha = 0^\circ$	17
Figure 14: Lift coefficients variation with injection angle; $C\mu = 0.3$, $\alpha = 10^\circ$	18
Figure 15: Absolute changes in lift coefficients with injection angle; $C\mu = 0.3$, $\alpha = 10^\circ$	18
Figure 16: Relative changes in lift coefficients with injection angle; $C\mu = 0.3$, $\alpha = 10^\circ$	19
Figure 17: Drag coefficients variation with injection angle; $C\mu = 0.3$, $\alpha = 10^\circ$	19
Figure 18: Lift coefficients variation with injection angle; $C\mu = 0.2$, $\alpha = 0^\circ$	20
Figure 19: Absolute changes in lift coefficients with injection angle; $C\mu = 0.2$, $\alpha = 0^\circ$	20
Figure 20: Relative changes in lift coefficients with injection angle; $C\mu = 0.2$, $\alpha = 0^\circ$	21
Figure 21: Drag coefficients variation with injection angle; $C\mu = 0.2$, $\alpha = 0^\circ$	21
Figure 22: Lift coefficients variation with injection angle; $C\mu = 0.2$, $\alpha = 10^\circ$	22
Figure 23: Absolute changes in lift coefficients with injection angle; $C\mu = 0.2$, $\alpha = 10^\circ$	22
Figure 24: Relative changes in lift coefficients with injection angle; $C\mu = 0.2$, $\alpha = 10^\circ$	23
Figure 25: Drag coefficients variation with injection angle; $C\mu = 0.2$, $\alpha = 10^\circ$	23
Figure 26: Lift coefficients variation with injection angle; $C\mu = 0.1$, $\alpha = 0^\circ$	24
Figure 27: Absolute changes in lift coefficients with injection angle; $C\mu = 0.1$, $\alpha = 0^\circ$	24
Figure 28: Relative changes in lift coefficients with injection angle; $C\mu = 0.1$, $\alpha = 0^\circ$	25
Figure 29: Drag coefficients variation with injection angle; $C\mu = 0.1$, $\alpha = 0^\circ$	25
Figure 30: Lift coefficients variation with injection angle; $C\mu = 0.1$, $\alpha = 10^\circ$	26
Figure 31: Absolute changes in lift coefficients with injection angle; $C\mu = 0.1$, $\alpha = 10^\circ$	27
Figure 32: Relative changes in lift coefficients with injection angle; $C\mu = 0.1$, $\alpha = 10^\circ$	27
Figure 33: Drag coefficients variation with injection angle; $C\mu = 0.1$, $\alpha = 10^\circ$	27

Figure 34: Lift coefficients variation with injection angle; $C\mu = 0.1$, $\alpha = 10^\circ$	28
Figure 35: Drag coefficients variation with injection angle; $C\mu = 0.1$, $\alpha = 10^\circ$	29
Figure 36: Streamlines and velocity vectors for 10° to 60° injection angles at 5% chord length location when $C\mu = 0.1$ and $\alpha = 10^\circ$	30
Figure 37: Streamlines and velocity vectors for 10° to 60° injection angles at 15% chord length location when $C\mu = 0.1$ and $\alpha = 10^\circ$	31
Figure 38: Streamlines and velocity vectors for 60° injection angles at 5% chord length location when $C\mu = 0.1$ and $\alpha = 10^\circ$	32
Figure 39: Streamlines and velocity vectors for 60° injection angles at 15% chord length location when $C\mu = 0.1$ and $\alpha = 10^\circ$	32
Figure 40: Streamlines and velocity vectors for 60° injection angles at 25% chord length location when $C\mu = 0.1$ and $\alpha = 10^\circ$	33
Figure 41: Stall angle analysis when injection slot is at 5% chord length location and injection angle is 0°	36
Figure 42: Stall angle analysis when injection slot is at 5% chord length location and injection angle is 40°	37
Figure 43: Stall angle analysis when injection slot is at 15% chord length location and injection angle is 0°	38
Figure 44: Stall angle analysis when injection slot is at 15% chord length location and injection angle is 40°	39

List of Tables

Table 1: Geometry parameters for CFJ airfoil with changeable injection angle.	15
Table 2: Geometry parameters for stall angle analysis.	34

Nomenclature

AoA	=	<i>Angle of Attack</i>
CFJ	=	<i>Co-Flow Jet</i>
RANS	=	<i>Reynolds-Averaged Navier-Stokes</i>
F_{xcfj}	=	<i>the reactionary force generated by the jet ducts in x direction</i>
F_{ycfj}	=	<i>the reactionary force generated by the jet ducts in y direction</i>
\dot{m}_j	=	<i>the mass flow</i>
V_j	=	<i>the injection flow velocity</i>
p_j	=	<i>the static pressure at slot's exit</i>
A_j	=	<i>the area at slot's exit</i>
θ	=	<i>the angle between slot surface and the line normal to chord</i>
α	=	<i>the angle of attack</i>
β	=	<i>the injection angle</i>
D	=	<i>the drag</i>
L	=	<i>the lift</i>
R'_x	=	<i>the surface integral of pressure and shear stress in drag direction</i>
R'_y	=	<i>the surface integral of pressure and shear stress in lift direction</i>
C_μ	=	<i>the jet momentum coefficient, $C_\mu = \frac{\dot{m}_j V_j}{\frac{1}{2} \rho_\infty V_\infty^2 S}$</i>
ρ_∞	=	<i>the far field free stream density</i>
V_∞	=	<i>the far field free stream velocity</i>
S	=	<i>the platform area of the airfoil</i>

c	=	<i>the chord length</i>
ρ_j	=	<i>the injection slot flow density</i>
$P_{t_{inj}}$	=	<i>the injection slot inlet total pressure</i>
$P_{s_{inj}}$	=	<i>the suction slot exit static pressure</i>
Re	=	<i>Reynolds Number</i>
Cl	=	<i>the lift coefficient</i>
Cd	=	<i>the drag coefficient</i>
L.E.	=	<i>leading edge</i>

Acknowledgments

I would like to express my deepest gratitude to those who helped me during my research in computation fluid dynamics lab at Washington University in St. Louis.

My deepest gratitude goes first and foremost to Professor Ramesh Agarwal for his encouragement and guidance throughout my research. His knowledge, experience and guidance has helped me to accomplish my entire research and thesis in reasonable steps. Without him I won't have the opportunity to explore the academic world of computation fluid dynamics.

Second, I would like to express my heartfelt gratitude to Dr. Han Gao and Dr. Qiongyao Qing for all the effort they put in to help me. The experienced idea about how to make researches of Dr. Han Gao helped me to start my research smoothly. And the careful guidance of Dr. Qiongyao Qing helped me to have the ability to conduct my research.

Finally, I would like to thank all the teachers, all the group members in computation fluid dynamics lab. It is the harmonious communication environment and exchanging of different ideas that let me keep learning and progress.

Da Xiao

Washington University in St. Louis

May 2019

Dedication

I would like to dedicate this thesis to my father (Haizhou Xiao) and my mother (Guihua Yang)
for their unconditional support.

I will never succeed without their guidance, influence and encouragement.

ABSTRACT OF THE THESIS

Numerical Simulation of Flow Past NACA 0012 Airfoil Using a Co-Flow Jet at Different

Injection Angles to Control Lift and Drag

by

Da Xiao

Master of Science in Mechanical Engineering

Washington University in St. Louis, 2019

Research Advisor: Professor Ramesh K. Agarwal

The focus of this thesis is to numerically study the aerodynamic performance of an airfoil by employing the active flow control from a co-flow jet (CFJ) near the leading edge. The study is conducted by changing the injection angle of CFJ on a location close to the leading edge on the upper surface of a most widely used NACA 0012 airfoil. The compressible Reynolds-Averaged Navier-Stokes (RANS) equations with Spalart-Allmaras (SA) turbulence model are solved using the commercial CFD solver ANSYS FLUENT. Steady state solver is employed in the simulations with pseudo-transient numerical method. The study is performed at free stream angles of attack from 0° and 10° for momentum coefficients $C_\mu = 0.1, 0.2$ and 0.3 with injection slot located at 5%, 15% and 25% chord length from the leading edge of the airfoil. It is shown that for given free stream conditions, the lift coefficient can be substantially increased and drag coefficient can be decreased with suitable choice of C_μ , injection angle and location of co-flow jet on the airfoil surface and different injection angles can have different aerodynamic coefficients performance. Thus, Changeable Injection Angle CFJ technology can be used for

AFC to achieve the desired outcome of increasing the lift of an airfoil, decreasing drag of an airfoil and at the same time, to have a control of aerodynamic coefficients.

Chapter 1: Introduction

Co-Flow Jet (CFJ) concept is a recently developed flow control (FC) method developed by Zha et al. [1-11] that can significantly improve airfoil performance. CFJ is different from traditional FC [12-18] as shown in Figure 2. This CFJ control method is implemented on an airfoil by opening an injection slot near the leading edge (LE) and a suction slot near the trailing edge (TE) on the airfoil upper surface. A small amount of mass is drawn into the suction slot and then pressurized and energized by a pumping system inside the airfoil. After pressurization, the flow is ejected from the injection slot and forms a co-flow jet tangentially on the upper surface of the airfoil. The whole CFJ process does not add any extra mass flow into the system and hence is a zero-net mass-flux flow control.

Compared to the baseline airfoil, CFJ airfoil can drastically increase lift and stall margin, and reduce drag. The fundamental concept is that by changing the circulation, aerodynamic forces can be changed. The turbulent mixing between the jet and the main flow energizes the wall boundary-layer and thus increases the circulation which results in lift augmentation. In addition, the total drag is also reduced as there is a thrust generated and the wake velocity deficit is reduced. Figure 1 shows the difference in streamline patterns around the airfoil between the baseline airfoil and the CFJ airfoil. Compared to the traditional FC airfoil, CFJ has an advantage since it is a zero-net mass flux control that requiring no intake of air from other sources such as engine of an airplane. It is like a zero net mass-flux synthetic jet actuator but has higher control authority and therefore is more effective. Also, as shown in Figure 2, CFJ airfoil nearly has no wake while FC airfoil still has some limited wake which implies that the CFJ airfoil with both injection and suction can provide stronger mixing and energy transfer [5, 6, 11].

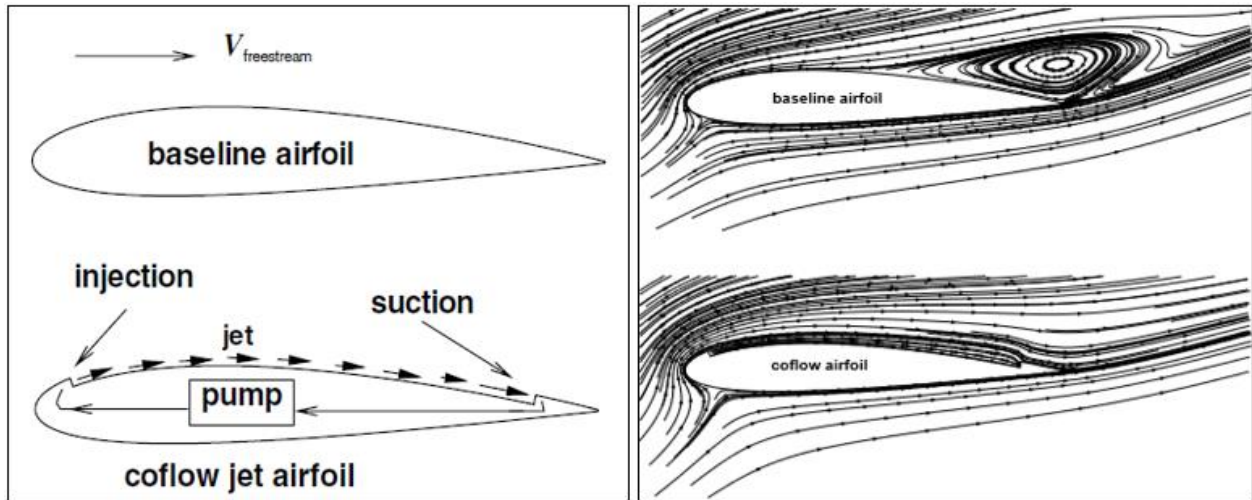


Figure 1: CFJ and baseline airfoil.

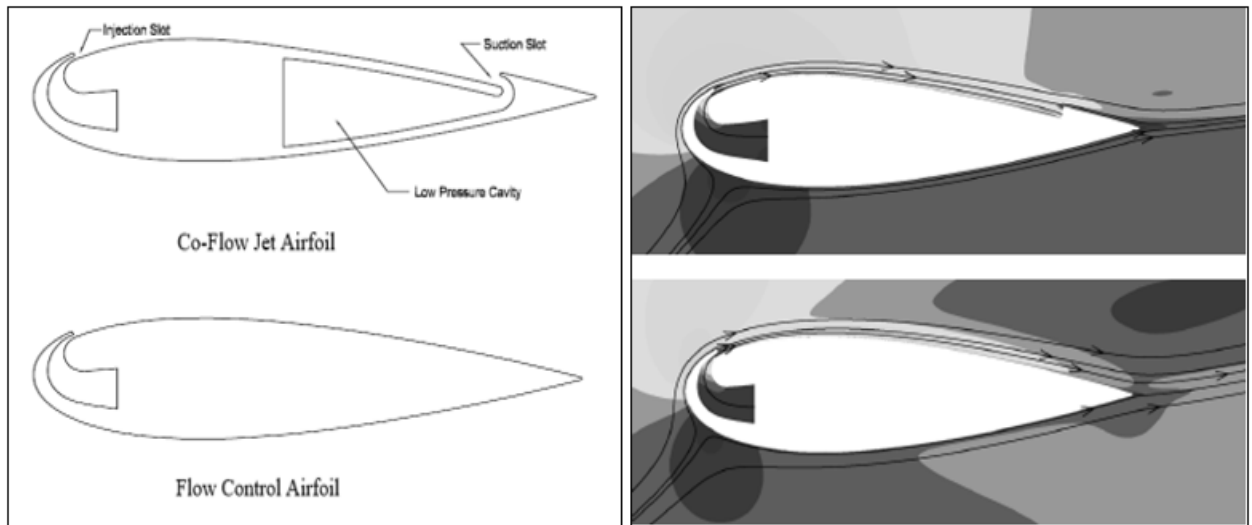


Figure 2: CFJ and FC airfoil.

The study in this thesis is based on CFJ airfoil technology. The research already developed by Zha et al. is mainly deals with tangential CFJ flow. This thesis introduces changeable injection angle concept into the CFJ technology. Changeable injection angle method can create different characteristic in the flow on the upper surface of the airfoil to modulate both lift and drag. The study is based on NACA0012 airfoil. By changing the injection angle of the injection jet of different jet momentum coefficients C_{μ} with different injection locations, this thesis tries to

determine the influence of an injection CFJ on aerodynamic coefficients by changing it C_{μ} , injection location and injection angle.

Chapter 2: CFJ Parameters

This section defines the important parameters that are used to calculate the dependence of lift and drag of a NACA0012 CFJ airfoil by changing its C_μ , injection angle and injection location.

2.1 Lift and Drag Calculation

In addition to lift and drag on the airfoil due to free-stream flow, there are additional forces on the airfoil caused by the momentum of the injection jet at the injection slot and suction at the suction slot for the CFJ airfoil. These additional forces are automatically included in the measurement of lift and drag in the wind tunnel. However, in a CFD simulation, ANSYS FLUENT cannot calculate the additional reactionary forces automatically. It can only calculate the forces acting on the surface of airfoil. Therefore, additional reactionary forces are included by using the control volume analysis. For CFJ airfoil without changeable injection angle, Zha et al. [6] give the following formulas Eq. (1) and Eq. (2) for calculating the reactionary forces by using the flow parameters at the injection and suction slots:

$$F_{xcfj} = (\dot{m}_j V_{j1} + p_{j1} A_{j1}) * \cos(\theta_1 - \alpha) - (\dot{m}_j V_{j2} + p_{j2} A_{j2}) * \cos(\theta_2 + \alpha) \quad (1)$$

$$F_{ycfj} = (\dot{m}_j V_{j1} + p_{j1} A_{j1}) * \sin(\theta_1 - \alpha) + (\dot{m}_j V_{j2} + p_{j2} A_{j2}) * \sin(\theta_2 + \alpha) \quad (2)$$

The subscripts 1 and 2 represent the injection and suction respectively. \dot{m}_j is the injection and suction mass flow (injection mass flow is equal to suction mass flow), V_j are injection and suction velocities, p_j are static pressures at two slots' exits, A_j are areas at two slots' exits and α is the angle of attack. θ_1 and θ_2 respectively are angles between the injection slot and suction slot and a line normal to the chord of airfoil.

This thesis introduces changeable injection angle β into the CFJ airfoil as shown in Figure 3.

Based on Figure 3, the formulas to calculate the reactionary forces become:

$$F_{xcfj} = (\dot{m}_j V_{j1} + p_{j1} A_{j1}) * \cos(\theta_1 + \beta - \alpha) - (\dot{m}_j V_{j2} + p_{j2} A_{j2}) * \cos(\theta_2 + \alpha) \quad (3)$$

$$F_{ycfj} = (\dot{m}_j V_{j1} + p_{j1} A_{j1}) * \sin(\theta_1 + \beta - \alpha) + (\dot{m}_j V_{j2} + p_{j2} A_{j2}) * \sin(\theta_2 + \alpha) \quad (4)$$

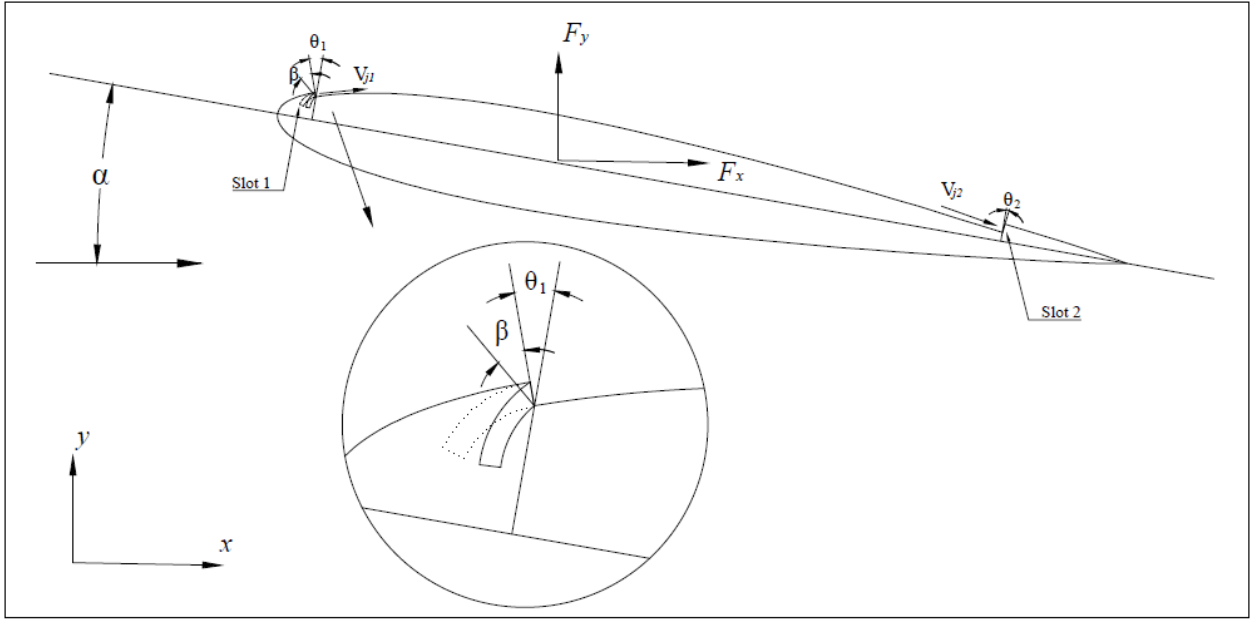


Figure 3: Flow parameters at the injection and suction slots.

The total lift and drag acting on the airfoil then can be expressed as:

$$D = R'_x - F_{xcfj} \quad (5)$$

$$L = R'_y - F_{ycfj} \quad (6)$$

R'_x and R'_y are the surface integral of pressure and shear stress in the drag and lift direction.

Thus, in the numerical simulation, the final drag and lift due to changeable injection angle on NACA0012 airfoil are calculated by the formulas given by Eq. (3), Eq. (4), Eq. (5) and Eq. (6).

2.2 Jet Momentum Coefficient

CFJ airfoil introduces a parameter called jet momentum coefficient C_μ to quantify the momentum of the injection jet. C_μ is defined as:

$$C_\mu = \frac{\dot{m}_j V_j}{\frac{1}{2} \rho_\infty V_\infty^2 S} \quad (7)$$

In Eq. (7), \dot{m}_j is injection mass flow, V_j is the injection velocity, ρ_∞ is far field free stream density, V_∞ is the far field free stream velocity and S is c , 1 meter. The c is the chord length of the airfoil and airfoil of unit span is assumed in non-dimensionalization of C_μ .

Chapter 3: Physical Model and Mesh

This section describes the flow conditions of the simulation as well as the geometry of the airfoil and structured mesh around it created in ICEM.

3.1 Flow Conditions

The flow past a changeable injection angle CFJ NACA0012 airfoil of chord length $c = 1.0 \text{ m}$ is investigated. The Mach number is 0.2 and Reynolds number is about 4,564,760. Angle of attack, jet momentum coefficient, injection angle and injection slot location are changed in different cases as shown in Table 1 and Table 2 in section 6.1 and section 6.3 respectively.

3.2 Geometry and Mesh

A C-block computational domain is used as shown in Figure 4. The maximum horizontal length of the domain is $35c$ ($20c$ in front of the airfoil and $14c$ behind the airfoil) so that the unbounded flow condition can be satisfied during the calculation. Figure 4 also show the structured mesh with refinements near the injection slot and suction slot and in the wake region. The suction slot in all cases is located at 85% chord length but the injection slots are located at 5% chord length, 15% chord length, 25% chord length on the upper surface of the airfoil for different cases as shown in Figure 5. Injection angle changes from 0° to 50° for different cases at each injection slot location as shown in Figure 6. The chord length is 1m, injection slot width is 0.005m and suction slot width is 0.01m. There are 306,750 nodes in the computational domain and the first layer cell height on the airfoil surface is 0.0001m ensuring that $y^+ < 1$. The external boundary of the computational domain is set as a pressure far field condition.

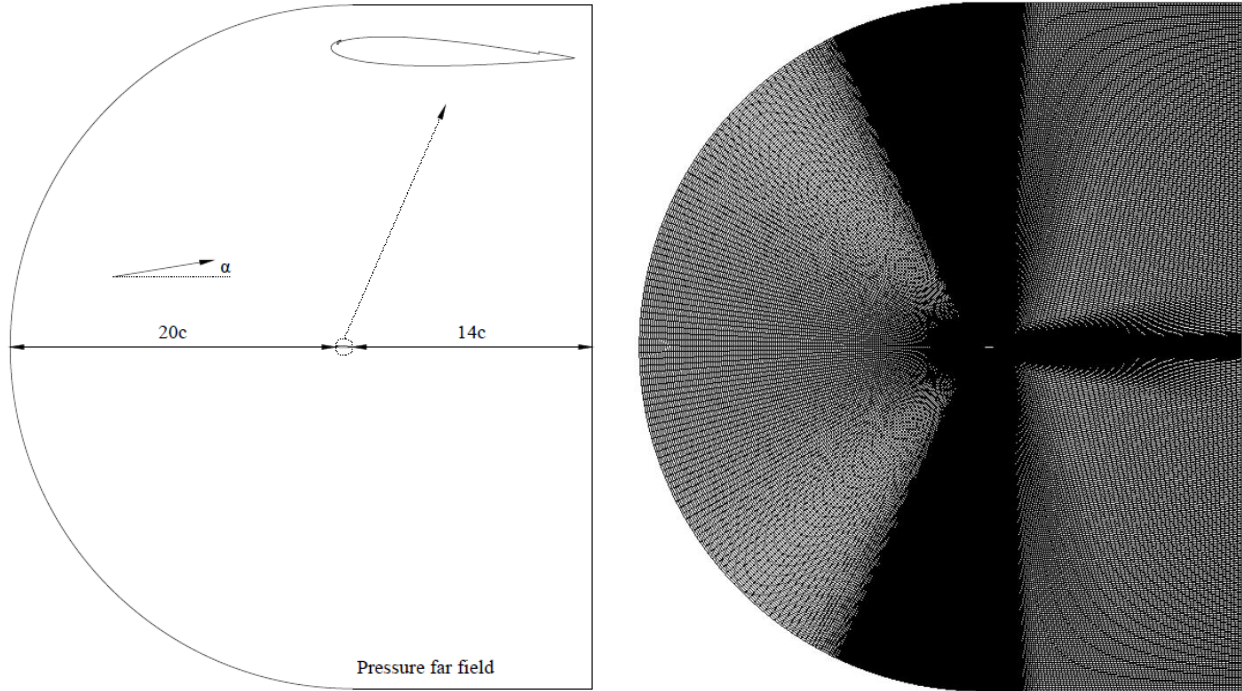


Figure 4: Computational domain and structured mesh.

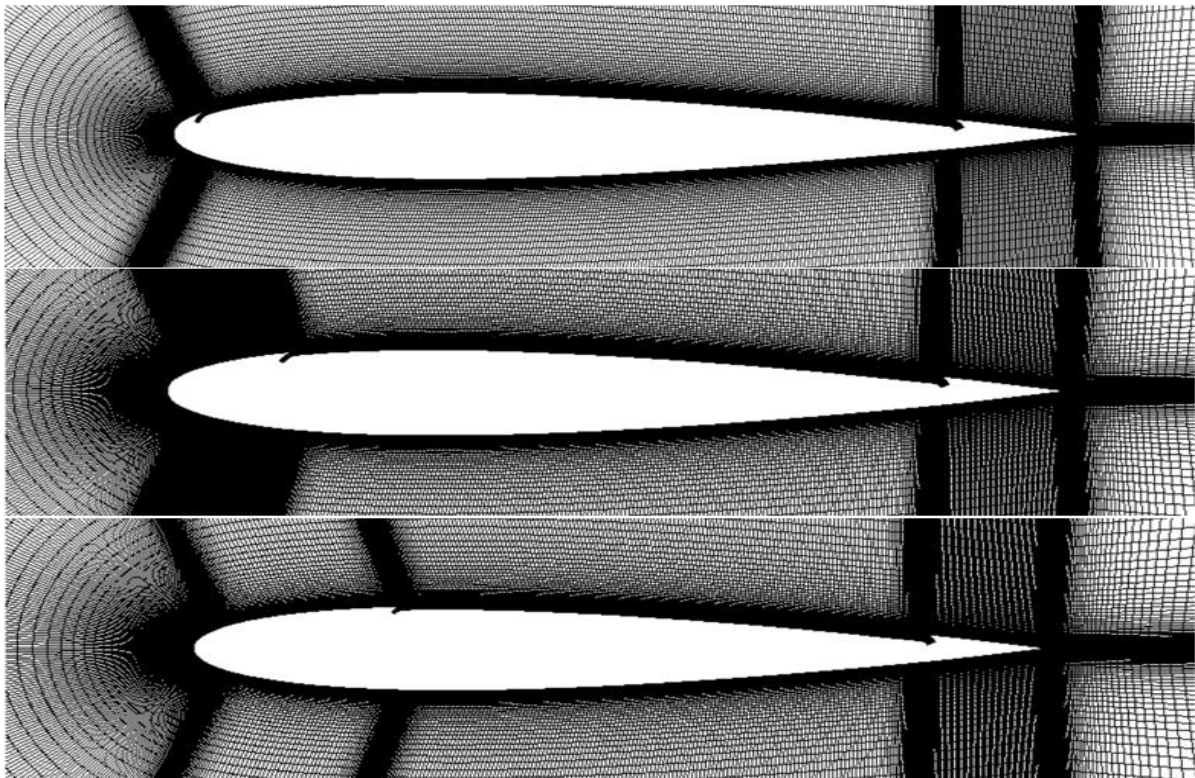


Figure 5: Refinement of the mesh near the changeable injection angle for CFJ NACA0012 airfoil.

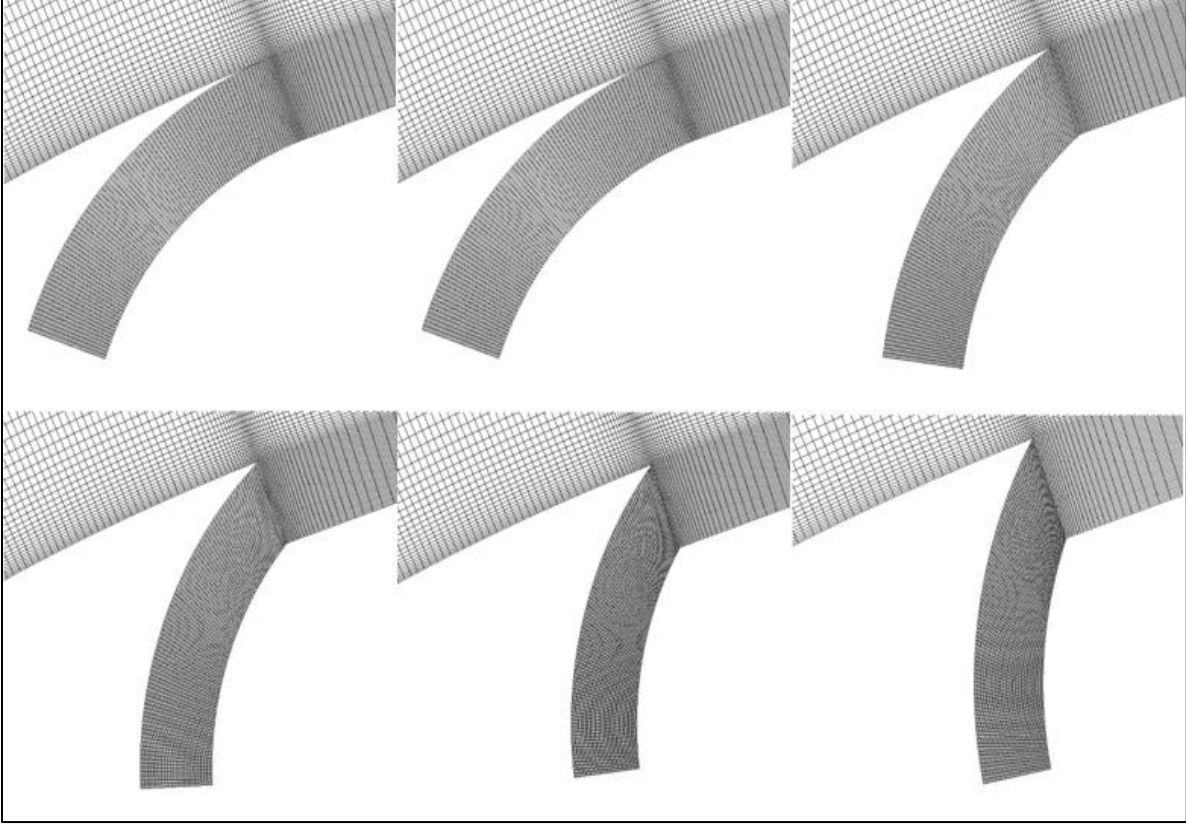


Figure 6: Changeable injection angle on the upper surface of the airfoil.

3.3 V_j with Different Injection Angles

V_j is a parameter that needs to be specified to calculate C_{μ} . In the simulation, V_j needs to be specified at injection slot exit curve 13 as shown in Figure 7 (a). In ANSYS FLUENT, curve 13 is set as a type of boundary condition called “interior” so that a UDF (user defined function) can extract necessary parameters at curve 13 to calculate V_j . There is no macro command in UDF that can directly extract velocity at an interior boundary condition. Because UDF has macro command to extract densities at first layer cells on interior boundary’s two sides, average density at curve 13 is known. Thus, injection velocity V_j can be obtained by the relation:

$$V_j = \frac{\dot{m}}{\rho_{j1} A_{j1} \cos \beta} \quad (8)$$

where mass flow \dot{m} can be extracted at curve 20 (pressure inlet boundary condition) and injection slot exit density ρ_{j1} can be extracted at curve 13 (interior boundary condition). As Figure 7 (b) shows, A_{j1} is the area at injection slot exit (curve 13) and $A_{j1} \cos \beta$ is the vertical cross section area of the injection slot (curve 17).

V_j changes with different injection angles β even when C_μ is the same.

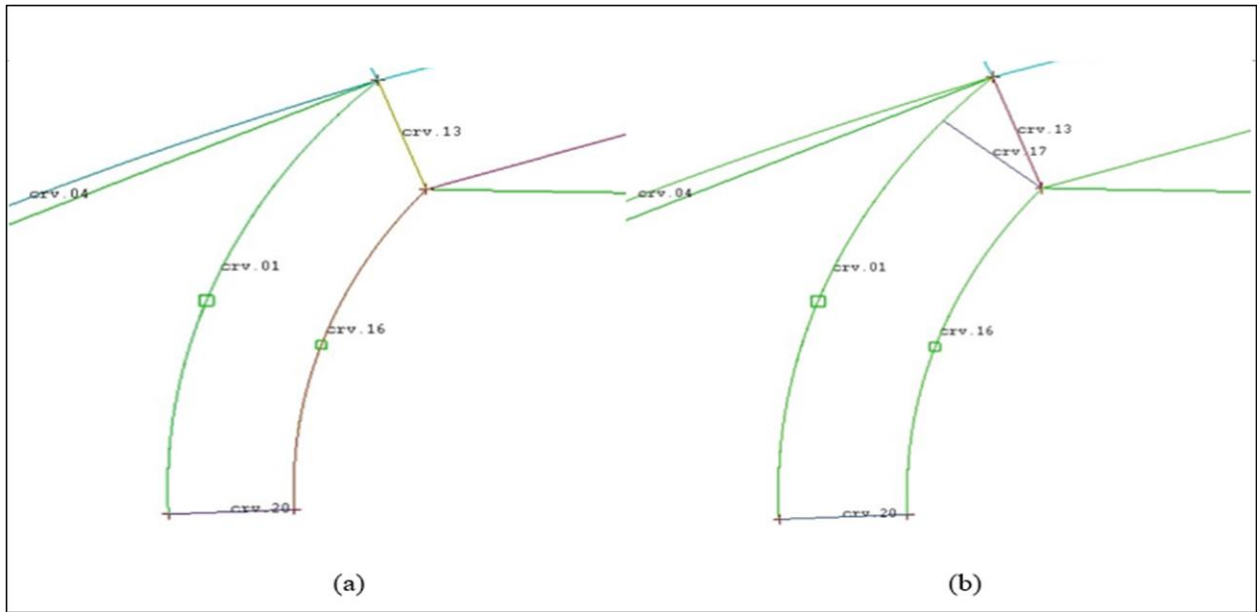


Figure 7: Diagrammatic sketch describing how to calculate V_j .

Figure 7 (a) shows the geometry used to create the mesh in ICEM and Figure 7 (b) is a diagrammatic sketch. There is no curve17 in the mesh geometry. Details about the UDF to satisfy a specific C_μ are given in next section and in Appendix.

Chapter 4: Numerical Method

This section describes the numerical set up employed in ANSYS FLUENT to achieve the simulations of CFJ NACA0012 airfoil using the changeable injection angles.

4.1 ANSYS FLUENT Setup and Boundary Conditions

The double precision solver in ANSYS FLUENT 17.1 is used to perform the CFD simulations. This research employs the 2D Compressible Reynolds-averaged Navier-Stokes equations with Spalart-Allmaras turbulence model. A Second-order numerical scheme is used for discretization of both the convection and diffusion terms. The pressure-coupled transient solver is used for pseudo-transient pressure-velocity coupling. Steady solver is employed in the simulations with pseudo-transient method. When results show a steady flow, convergence is considered achieved if lift coefficient and drag coefficient change within 0.01% over 1000 iterations. When results show an unsteady flow, convergence is considered achieved if lift coefficient and drag coefficient become periodic after several cycles and do not change from one cycle to next cycle; 20 cycles are chosen as the time average period to calculate the average aerodynamic coefficients for the unsteady periodic flow.

No slip wall condition is used on the airfoil solid surface and on the injection and suction slot two side walls. Pressure-far-field condition with Mach number = 0.2 and total pressure = 0 are set to satisfy the far-field unbounded flow boundary conditions at the outer boundary of the computational domain. The inlet of injection slot is set as pressure inlet condition with changeable total pressure controlled by UDF. The exit of suction slot is set as a pressure outlet condition with changeable static pressure controlled by UDF. The operating condition is one standard atmospheric pressure.

4.2 UDF of C_μ Iteration

CFJ airfoil must achieve zero net mass flux under all operating conditions. The mass flow exiting from injection slot \dot{m}_{inj} must be equal to the mass flow entering the suction slot \dot{m}_{suc} . The momentum of the flow is defined by C_μ and a specific value of C_μ is achieved by adjusting the injection slot inlet total pressure $P_{t_{inj}}$. The \dot{m}_{suc} matches \dot{m}_{inj} by adjusting the suction slot exit static pressure $P_{s_{suc}}$. During each iteration, there is a UDF process to judge whether the above two conditions are achieved by adjusting the $P_{t_{inj}}$ and $P_{s_{suc}}$ automatically. The acceptable variation for C_μ and mass flow are both within 0.2% for this research.

Chapter 5: Validation of Numerical Method

The numerical investigation of the flow field of NACA0012 airfoil at Reynolds number of $Re = 6 \times 10^6$ at angle of attack is 10° and chord length is 1 meter is conducted to validate the numerical method in ANSYS FLUENT. The pressure coefficient C_p is plotted against x/c in Figure 8. The experimental results are from Gregory and O'Reilly [19].

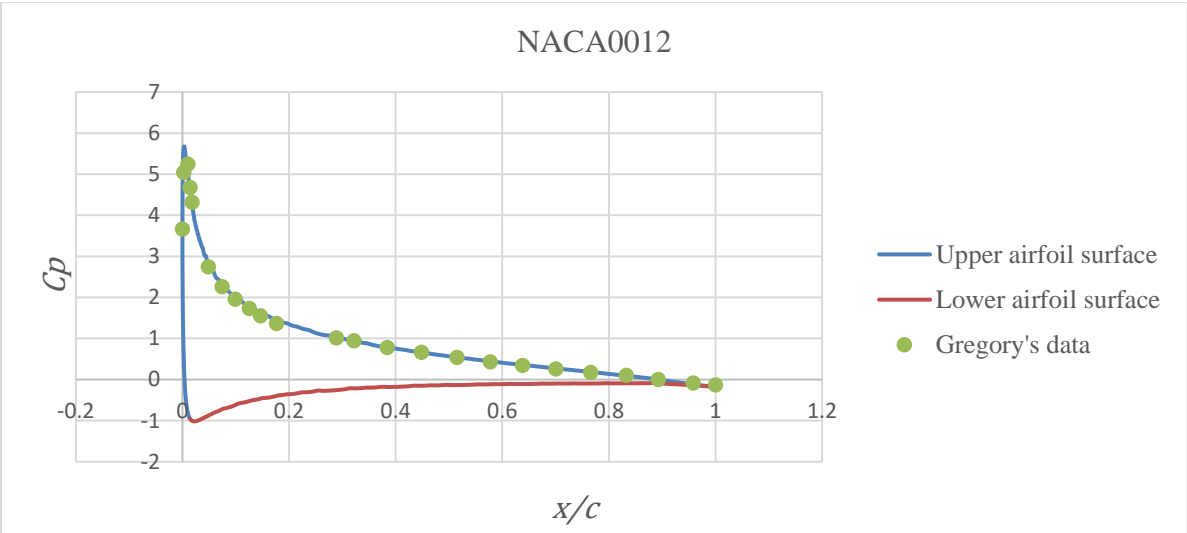


Figure 8: Pressure coefficient for flows past NACA0012 airfoil; $Re = 6 \times 10^6$, $\alpha = 10^\circ$.

The numerical results using the compressible RANS equations agree quite well with the experimental data as shown in Figure 8. The streamlines and velocity vectors are shown in Figure 9.

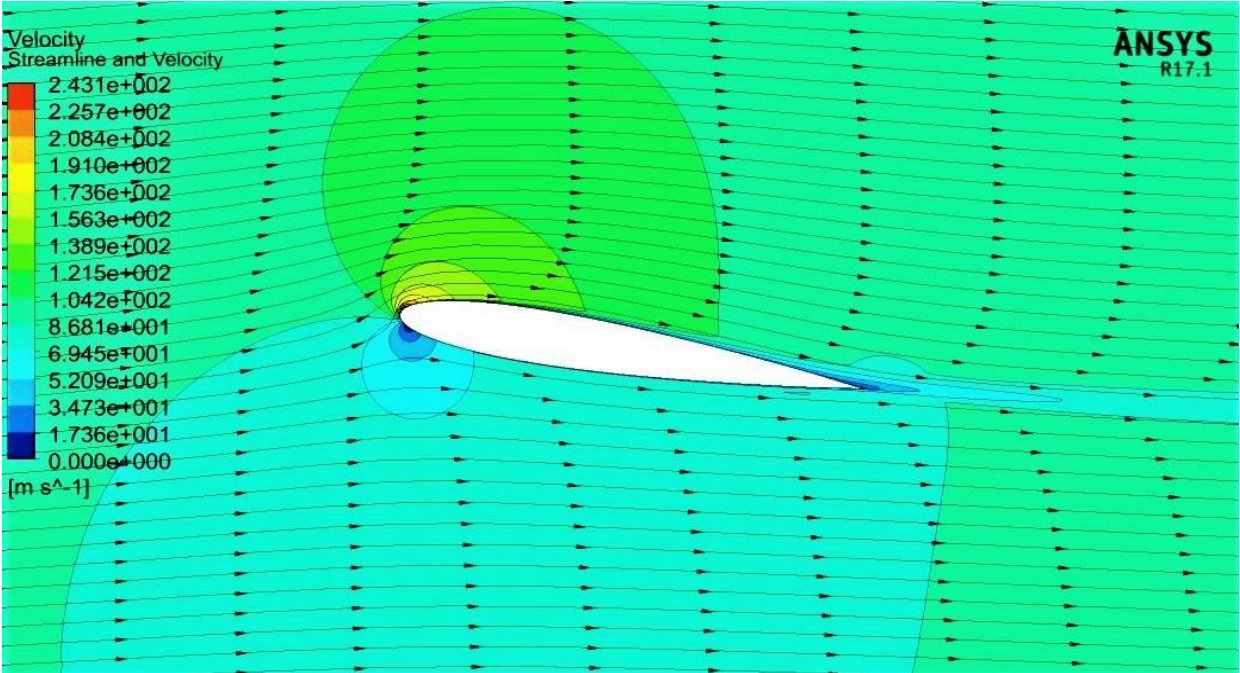


Figure 9: Streamlines and velocity vectors for flow past NACA0012 airfoil; $Re = 6 \times 10^6$, $\alpha = 10^\circ$.

Chapter 6: Results and Discussion

6.1 Changeable injection angle's influence on aerodynamic coefficients

As shown in Table 1, 18 different cases were computed and compared to study the influence of changeable injection angle on the aerodynamic coefficients with different C_{μ} , angle of attack and injection slot location. From these results, a best injection location can be determined by exercising control using the changeable injection angle CFJ.

Cases	C_{μ}	AoA	Injection slot location from L.E.	Injection angle
A1	0.1	0°	5%	0°, 10°, 20°, 30°, 40°, 50°
A2	0.1	0°	5%	
A3	0.1	0°	5%	
A4	0.2	0°	10%	
A5	0.2	0°	10%	
A6	0.2	0°	10%	
A7	0.3	0°	15%	
A8	0.3	0°	15%	
A9	0.3	0°	15%	
A10	0.1	10°	5%	
A11	0.1	10°	5%	
A12	0.1	10°	5%	
A13	0.2	10°	10%	
A14	0.2	10°	10%	
A15	0.2	10°	10%	
A16	0.3	10°	15%	
A17	0.3	10°	15%	
A18	0.3	10°	15%	

Table 1: Geometry parameters for CFJ airfoil with changeable injection angle.

Figures 10-13 show the results for cases A7, A8, A9 and Figure 14-17 show the results for cases A16, A17, A18. These figures show the change in aerodynamic coefficients with different injection angles when injection locations are different. Cases A7, A8, A9 and A16, A17, A18 are all computed for $C_{\mu} = 0.3$.

Figure 10 shows the variation in lift coefficient with injection angle for $C_{\mu} = 0.3$ and angle of attack = 0° . It shows that 5% and 15% chord length location of injection slot have nearly same lift coefficient with change in injection angle and their lift coefficients are all higher than these obtained for 25% chord length location of injection angle. Also, as injection angle becomes larger, the lift coefficient becomes smaller as expected. Figure 11 and Figure 12 show the absolute change and the relative change in lift coefficients at different injection angles compared to their respective tangential flow case. Figure 11 and Figure 12 show that when injection location is located at 15% chord length, the change in injection angle can produce most significant decrease in lift. The maximum decrease in lift can be 35% compared to its corresponding tangential flow case with absolute lift coefficient decreasing by 0.122.

Figure 13 shows that the drag coefficient increases when injection angle becomes larger. Also, the injection slot at 15% chord length location has the smallest drag coefficient.

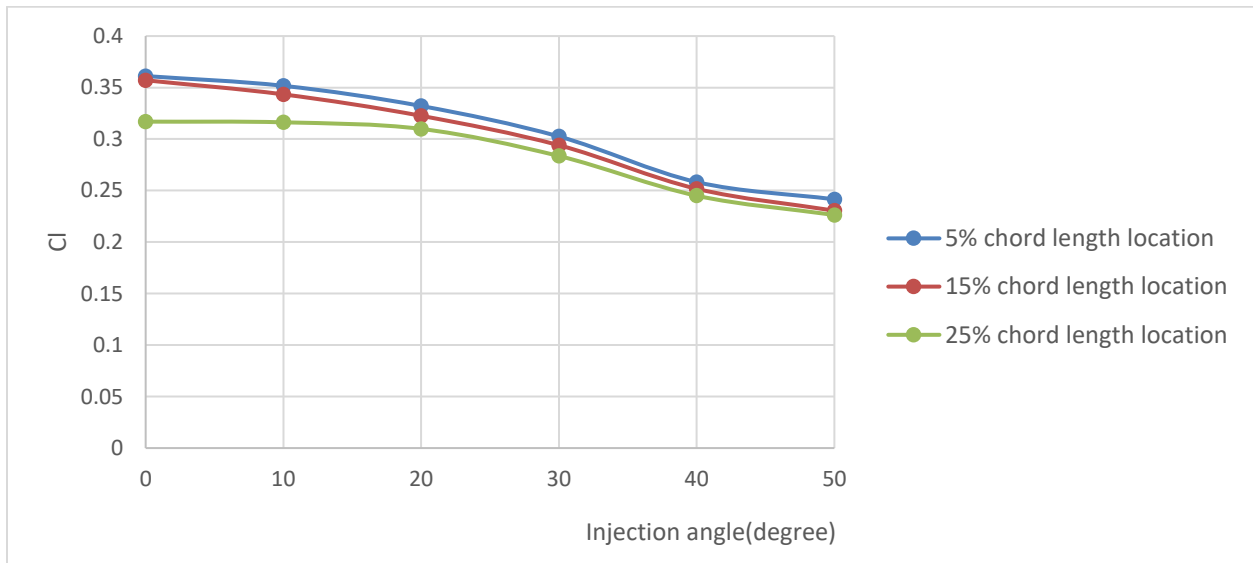


Figure 10: Lift coefficients variation with injection angle; $C_{\mu} = 0.3$, $\alpha = 0^{\circ}$.

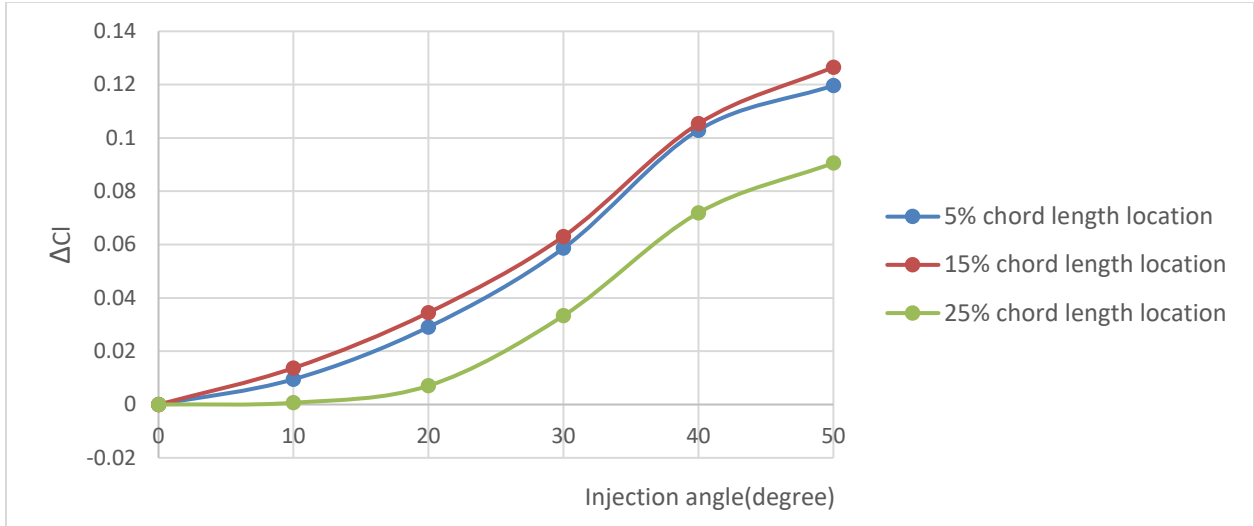


Figure 11: Absolute changes in lift coefficients with injection angle; $C_{\mu} = 0.3$, $\alpha = 0^{\circ}$.

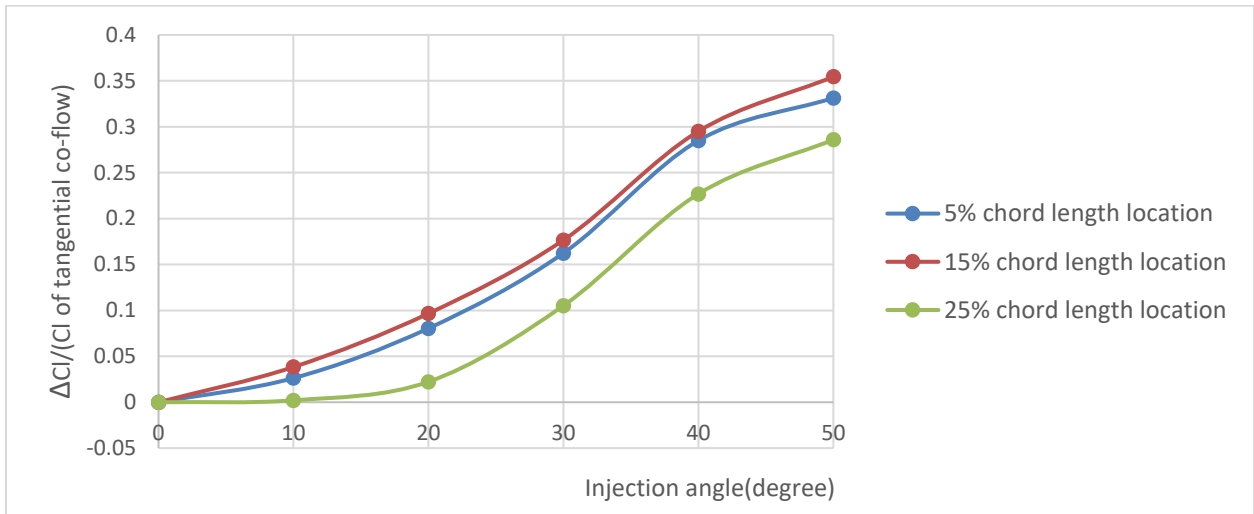


Figure 12: Relative changes in lift coefficients with injection angle; $C_{\mu} = 0.3$, $\alpha = 0^{\circ}$.

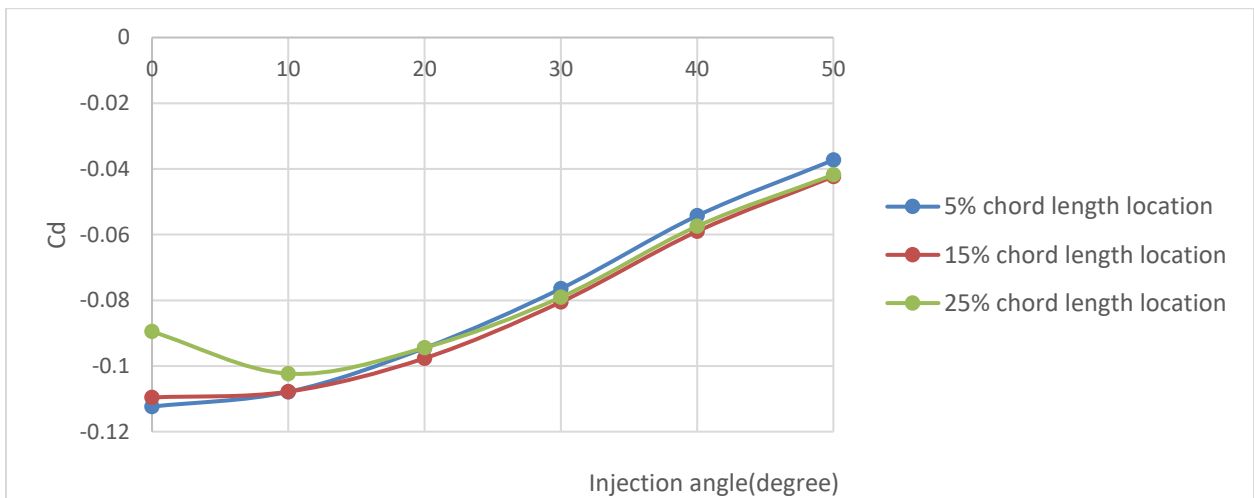


Figure 13: Drag coefficients variation with injection angle; $C_{\mu} = 0.3$, $\alpha = 0^{\circ}$.

Figures 14-17 show the results of computation when $\alpha = 0^\circ$ and $C_\mu = 0.3$. Figures 14-16 show that when injection slot is at 5% and 15% chord length location, the lift coefficients have nearly the same values and are all higher than that value at 25% chord length location of the injection slot. The decrease in maximum absolute lift coefficient is 0.2 and the decrease in maximum relative lift coefficient is 0.12. Thus, when the angle of attack becomes larger, the influence of change in injection angle on lift coefficient becomes relatively smaller.

Figure 17 shows that when injection slot is at 15% chord length location, the drag coefficient has minimum value. But as the injection angle becomes larger, drag coefficient increases.

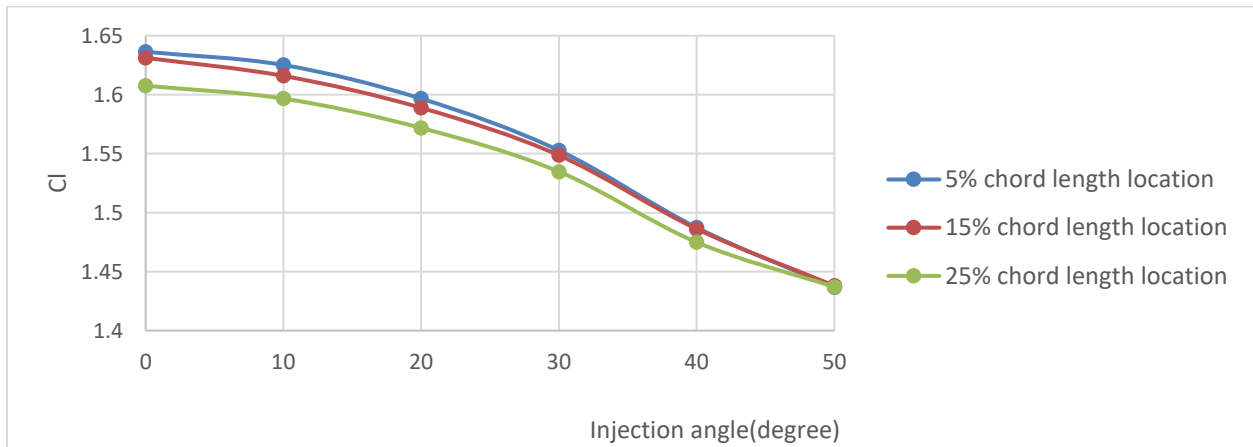


Figure 14: Lift coefficients variation with injection angle; $C_\mu = 0.3$, $\alpha = 10^\circ$.

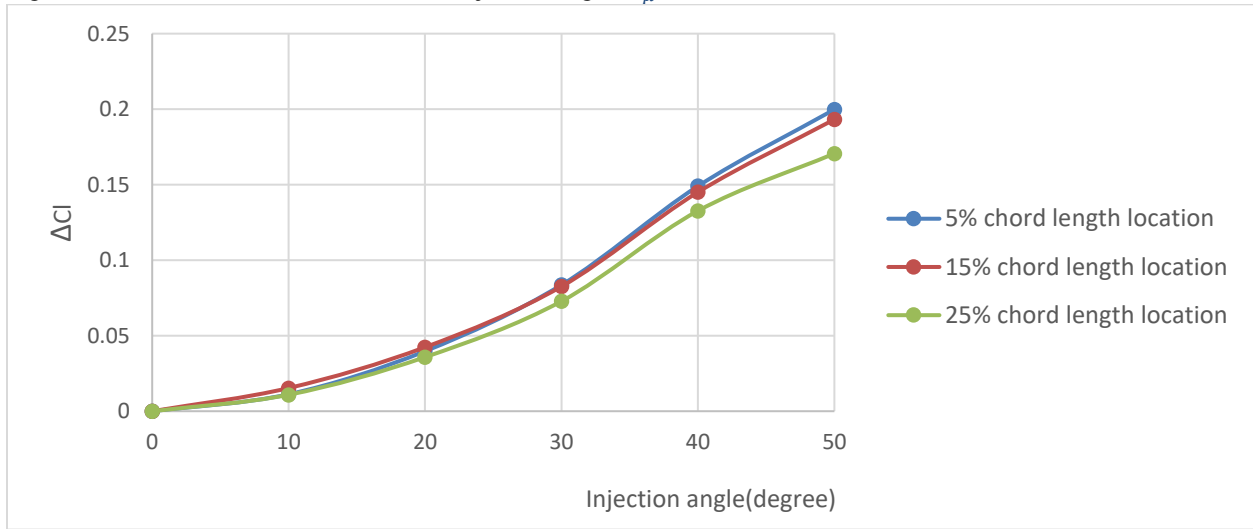


Figure 15: Absolute changes in lift coefficients with injection angle; $C_\mu = 0.3$, $\alpha = 10^\circ$.

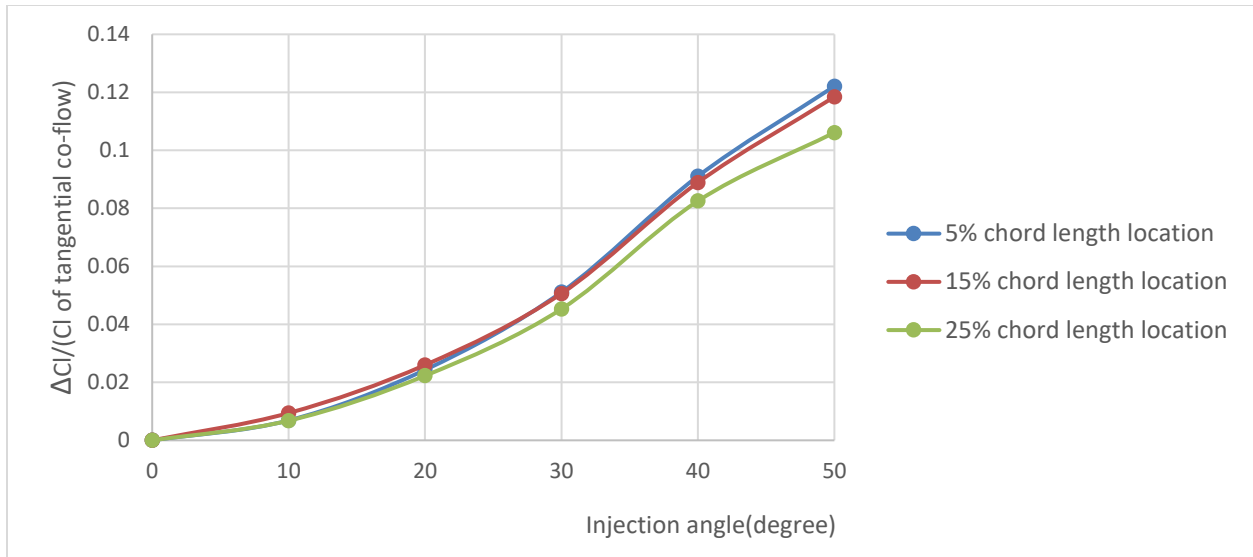


Figure 16: Relative changes in lift coefficients with injection angle; $C_\mu = 0.3$, $\alpha = 10^\circ$.

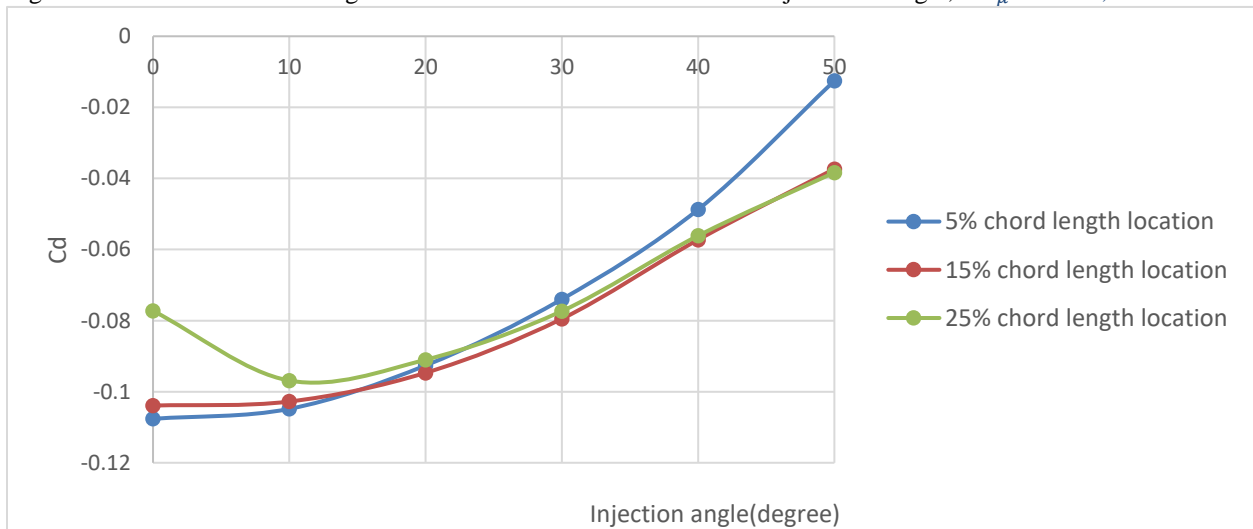


Figure 17: Drag coefficients variation with injection angle; $C_\mu = 0.3$, $\alpha = 10^\circ$.

Figures 18-21 show the results for A4, A5, A6 cases and the Figure 22-25 show the results for A13, A14, A15 cases. Cases A4, A5, A6 and A13, A14, A15 cases are computed with $C_\mu = 0.2$.

Figure 18 shows when $C_\mu = 0.2$ and $\alpha = 0^\circ$, the influence of changeable injection angle on lift coefficient is nearly the same at different injection locations. Since C_μ becomes smaller, all lift coefficients with different injection angles become smaller. From Figure 19 and Figure 20, changes in absolute lift coefficients and the relative lift coefficients also become smaller. When

$C_{\mu} = 0.2$ and $\alpha = 0^{\circ}$, 15% and 25% chord length locations of injection slot have higher changes in relative lift coefficients compared to 5% chord length location. At 15% chord length location of the injection slot, the maximum change in lift coefficient is about 25% and at 25% chord length location, the maximum change in lift coefficient is about 27%.

Figure 21 shows that at 5% and 15% chord length locations of injection slot, the drag coefficients become smaller than that at 25% chord length location of the injection slot and as the injection angle becomes larger, drag coefficient becomes larger.

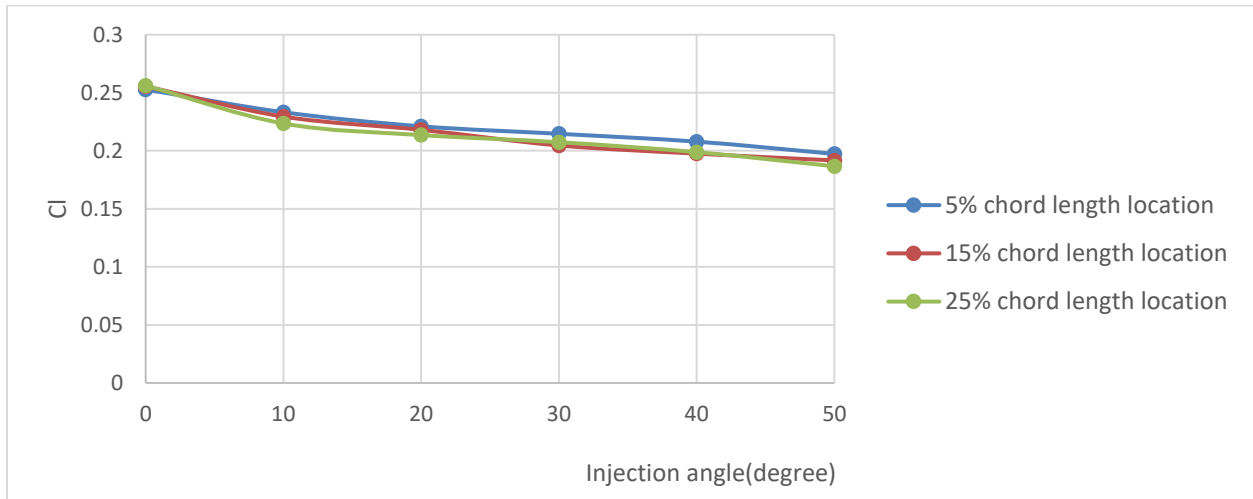


Figure 18: Lift coefficients variation with injection angle; $C_{\mu} = 0.2$, $\alpha = 0^{\circ}$.

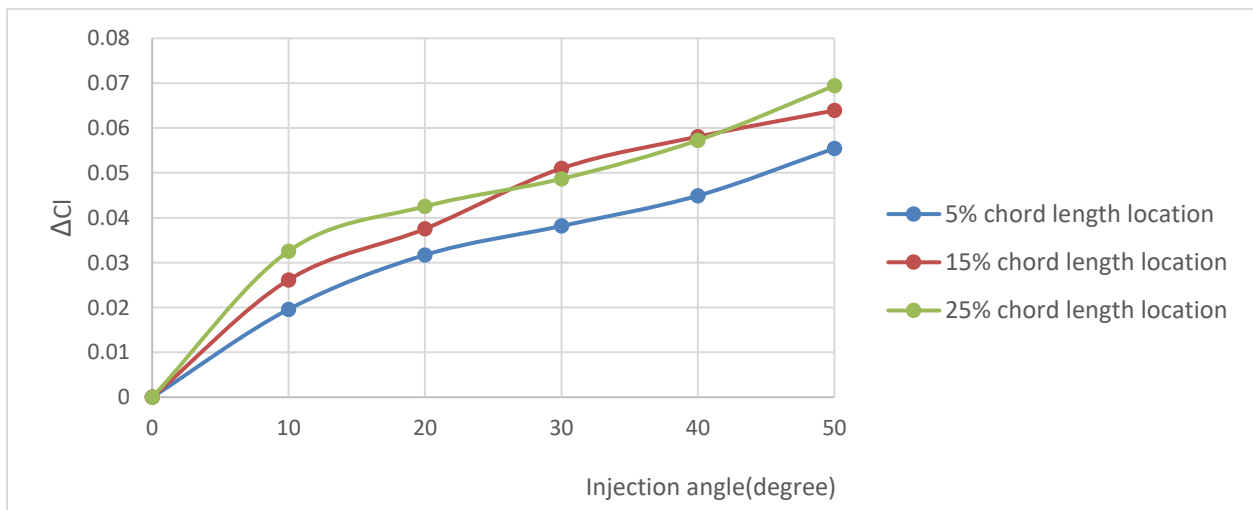


Figure 19: Absolute changes in lift coefficients with injection angle; $C_{\mu} = 0.2$, $\alpha = 0^{\circ}$.

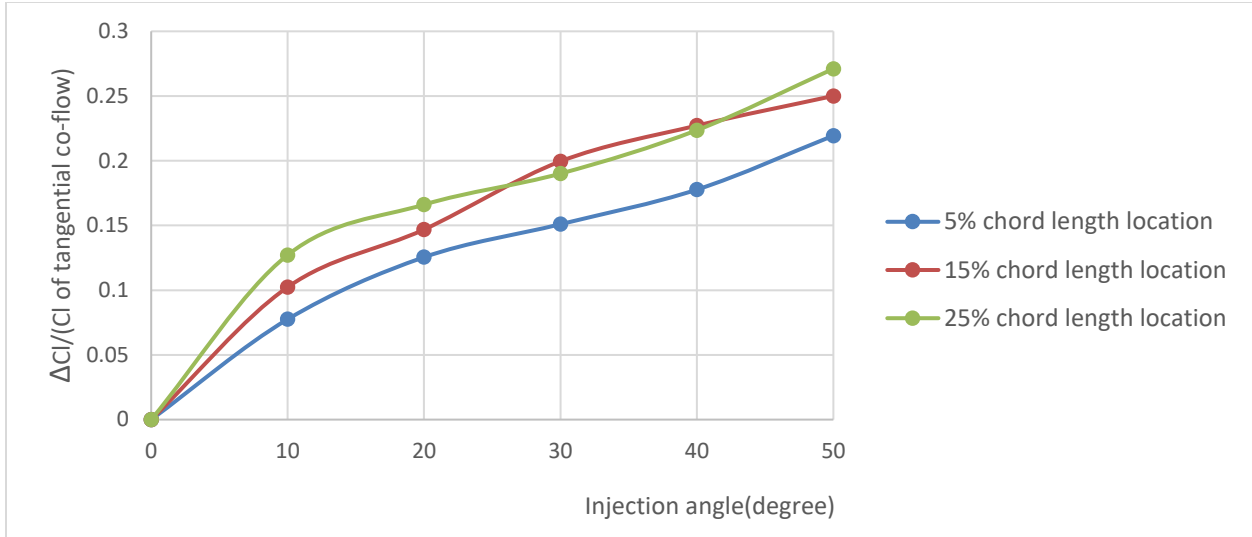


Figure 20: Relative changes in lift coefficients with injection angle; $C_{\mu} = 0.2, \alpha = 0^{\circ}$.

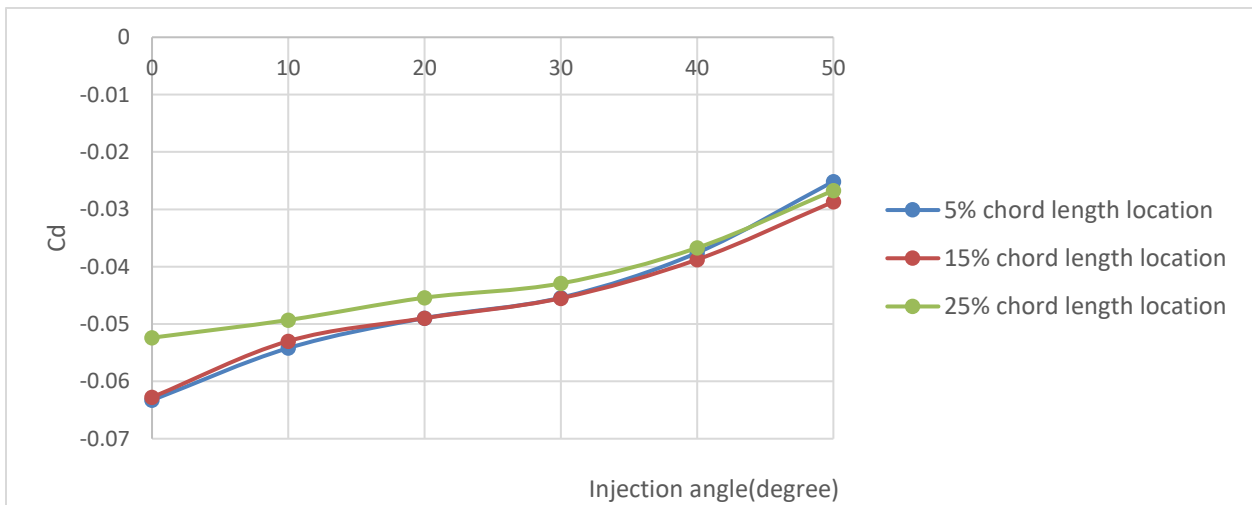


Figure 21: Drag coefficients variation with injection angle; $C_{\mu} = 0.2, \alpha = 0^{\circ}$.

Figures 22-24 show the lift coefficients, absolute changes in lift coefficients and relative changes in lift coefficients when $C_{\mu} = 0.2$ and $\alpha = 10^{\circ}$. At 15% chord length location of injection slot, the lift coefficients with different injection angle are larger than that for the 5% and 25% chord length location but the 15% chord length location has smaller relative changes in lift coefficients. When angle of attack becomes larger, the relative changes in lift coefficients

become smaller. When $C_{\mu} = 0.2$ and $\alpha = 10^\circ$, the maximum relative changes in lift coefficient at 5% chord length location of the injection slot is 5.5% and at 15% chord length location of the injection slot is 4.5%.

Figure 25 shows that the drag coefficients are smallest at 15% chord length location for different injection slot locations.

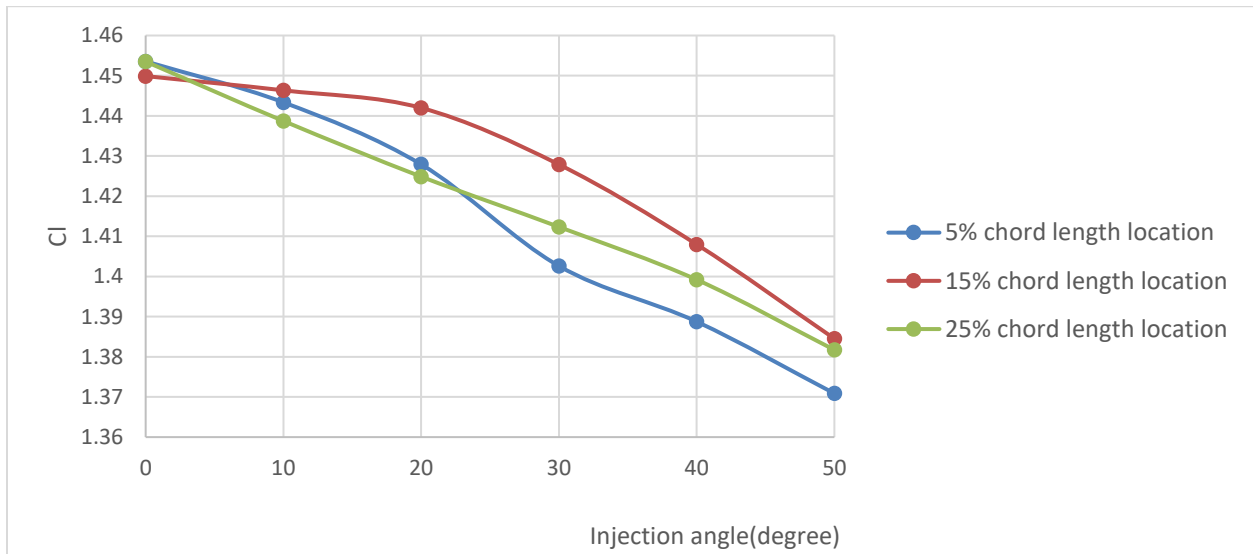


Figure 22: Lift coefficients variation with injection angle; $C_{\mu} = 0.2$, $\alpha = 10^\circ$.

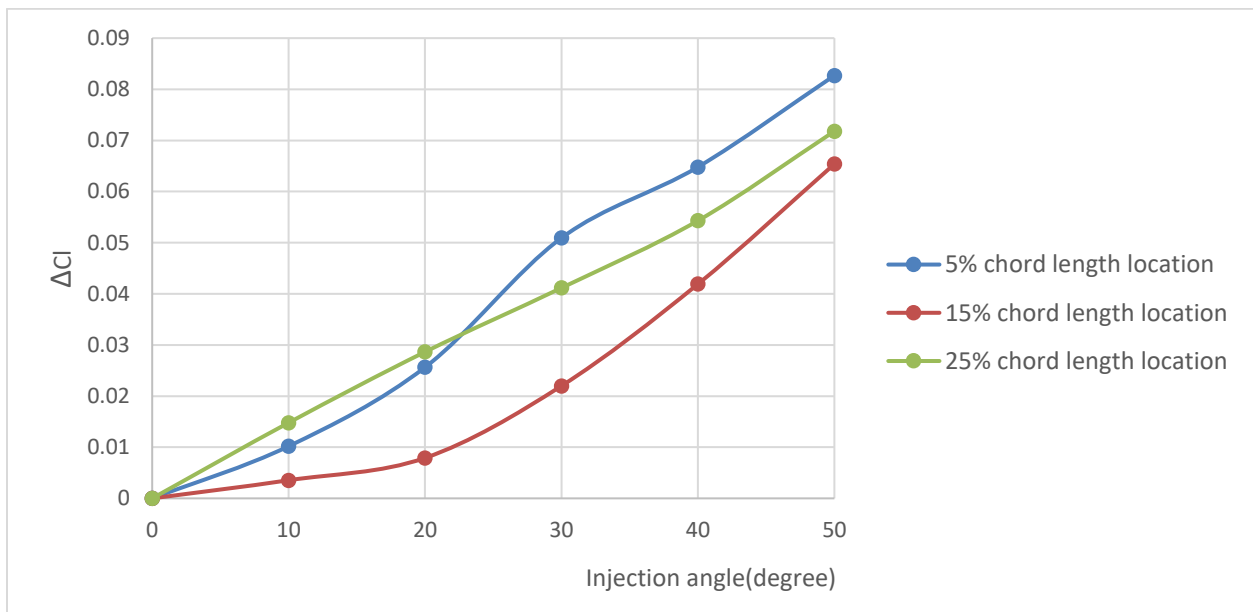


Figure 23: Absolute changes in lift coefficients with injection angle; $C_{\mu} = 0.2$, $\alpha = 10^\circ$.

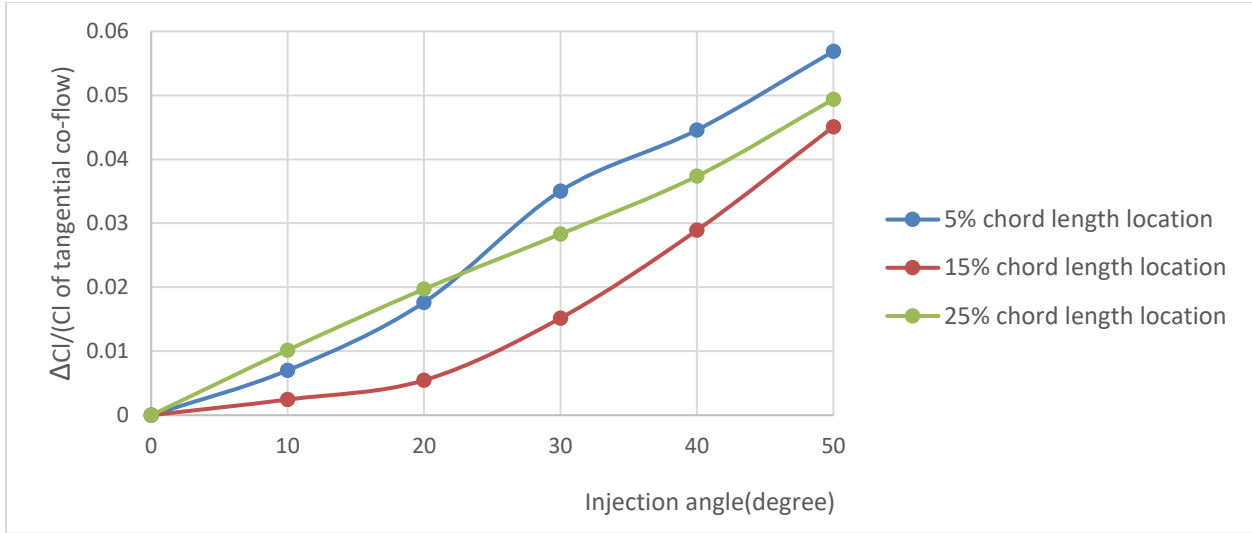


Figure 24: Relative changes in lift coefficients with injection angle; $C_\mu = 0.2$, $\alpha = 10^\circ$.

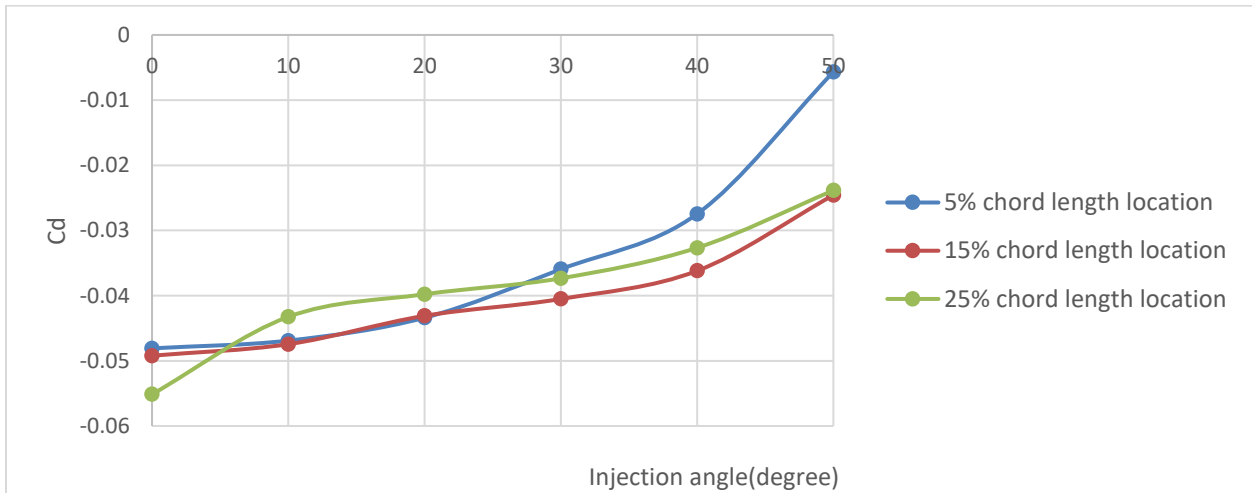


Figure 25: Drag coefficients variation with injection angle; $C_\mu = 0.2$, $\alpha = 10^\circ$.

Figures 26-29 show the results for A1, A2, A3 cases and Figures 30-33 show the results for A10, A11, A12 cases. Cases A1, A2, A3 and A10, A11, A12 are computed with $C_\mu = 0.1$.

Figure 18 shows that when $C_\mu = 0.1$ and $\alpha = 0^\circ$, the influence of changeable injection angle on lift coefficients is nearly the same at different locations of the injection slot. From Figures 27-28, the maximum absolute changes and relative changes in lift coefficient are at 15% and 25%

chord length location of the injection slot. Both the two locations have almost the same maximum relative change in lift coefficient which is about 25%.

Figure 29 shows that at 15% chord length location, the drag coefficients are always minimum among the three different locations of the injection slot with different injection angles when $C_{\mu} = 0.1$ and $\alpha = 0^{\circ}$.

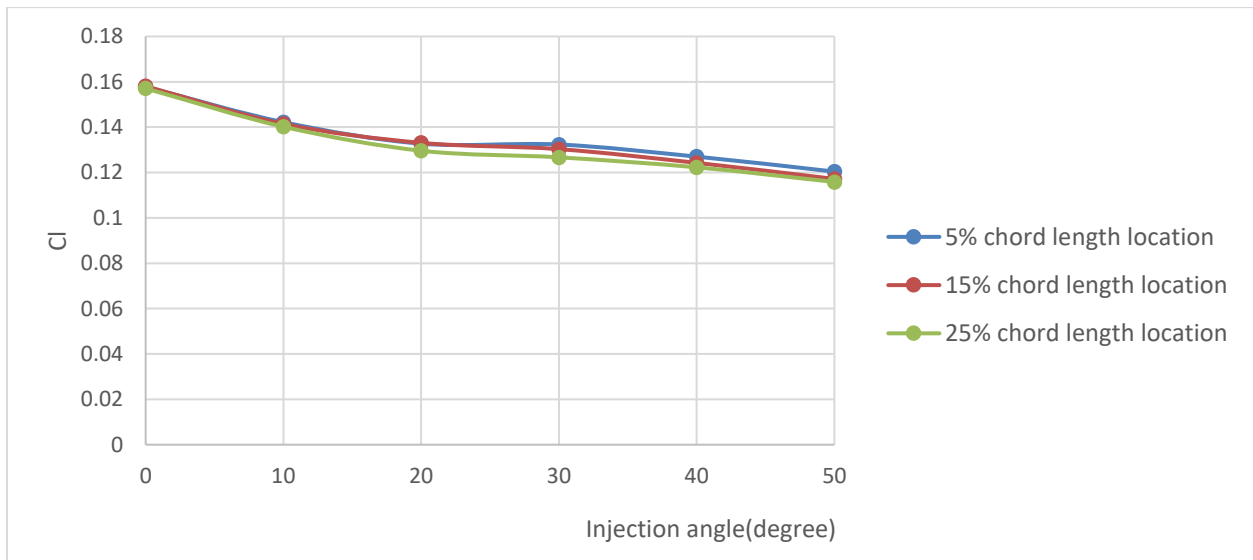


Figure 26: Lift coefficients variation with injection angle; $C_{\mu} = 0.1$, $\alpha = 0^{\circ}$.

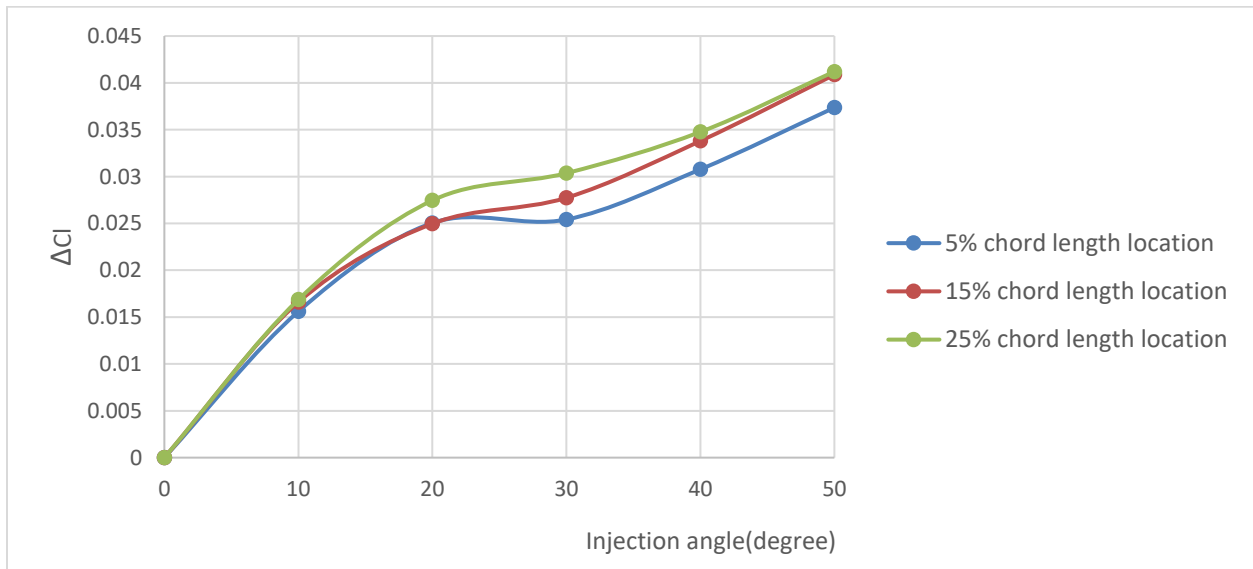


Figure 27: Absolute changes in lift coefficients with injection angle; $C_{\mu} = 0.1$, $\alpha = 0^{\circ}$.

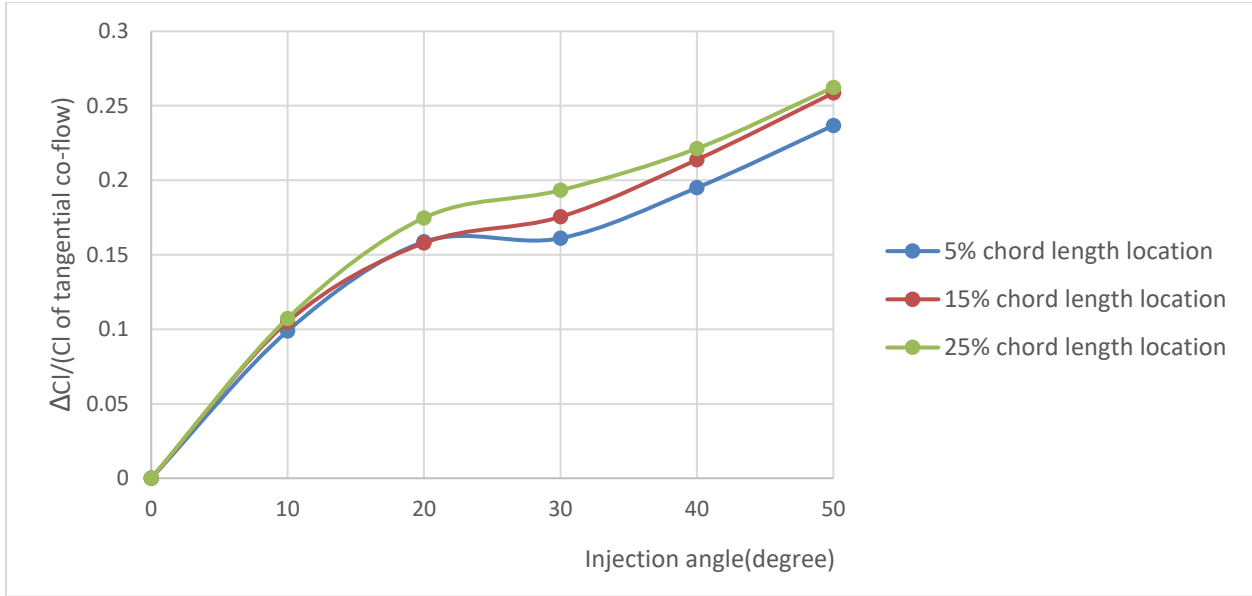


Figure 28: Relative changes in lift coefficients with injection angle; $C_{\mu} = 0.1$, $\alpha = 0^{\circ}$.

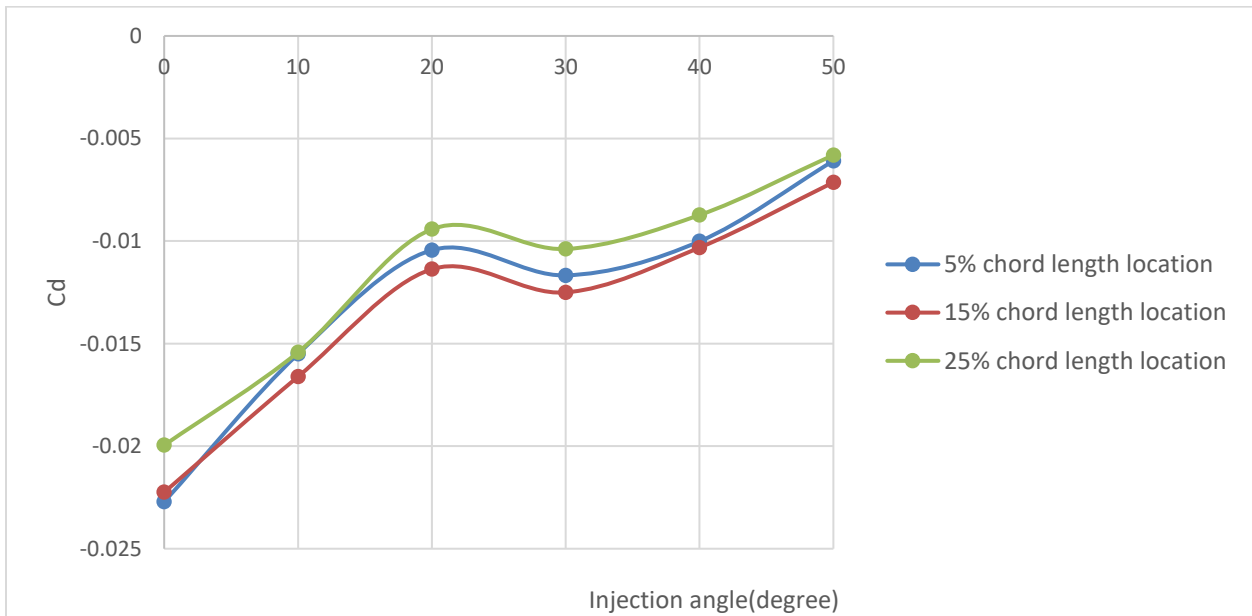


Figure 29: Drag coefficients variation with injection angle; $C_{\mu} = 0.1$, $\alpha = 0^{\circ}$.

Figures 30-33 show the results of aerodynamic coefficients that when $C_{\mu} = 0.1$ and $\alpha = 10^{\circ}$. When the injection angle becomes 50° , there are some sharp changes in aerodynamic coefficients with injection slot at 5% chord length location. The sharp changes are not desirable for changeable injection angle control. These sharp changes are described in next section.

From Figure 30, when the injection slot is located at 15% and 25% chord length location, lift coefficients have higher value compared to when the injection slot located at 5% chord length location. From Figure 31-32, the change in maximum absolute lift coefficient is about 0.06 and the change in maximum relative lift coefficient is about 5% (ignoring the sharp change at very high injection angle).

Figure 33 shows that when $C_{\mu} = 0.1$ and $\alpha = 10^\circ$, 15% chord length location has minimum drag coefficient among the three different injection slot locations.

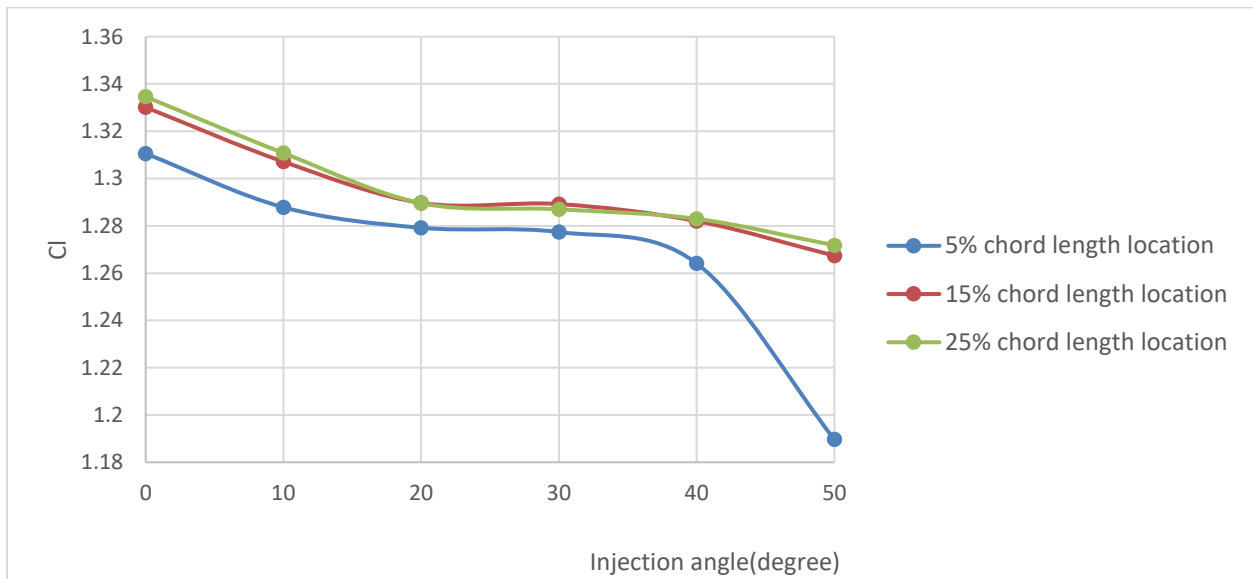


Figure 30: Lift coefficients variation with injection angle; $C_{\mu} = 0.1$, $\alpha = 10^\circ$.

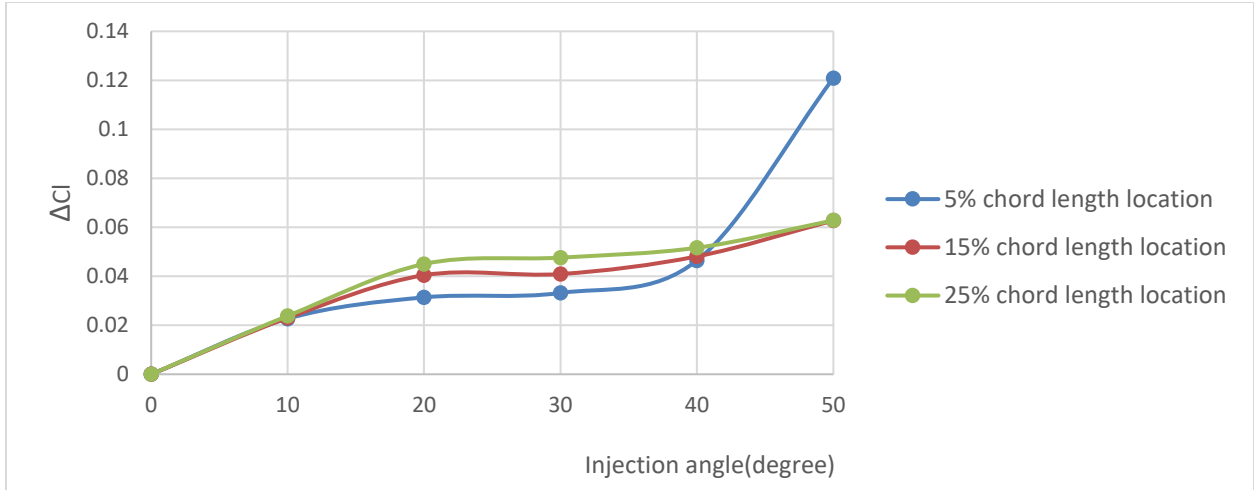


Figure 31: Absolute changes in lift coefficients with injection angle; $C_{\mu} = 0.1$, $\alpha = 10^{\circ}$.

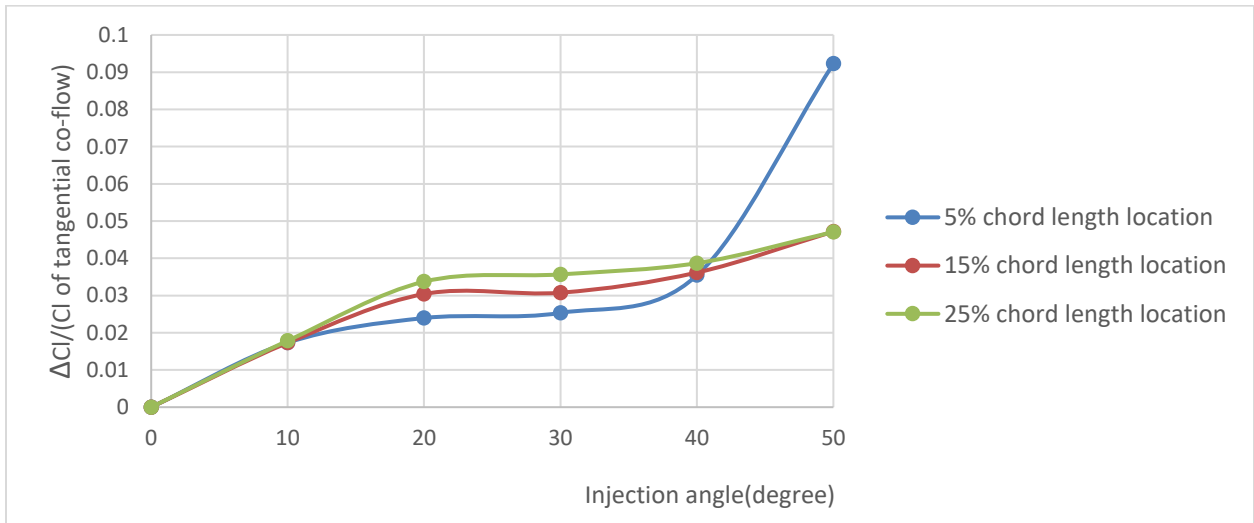


Figure 32: Relative changes in lift coefficients with injection angle; $C_{\mu} = 0.1$, $\alpha = 10^{\circ}$.

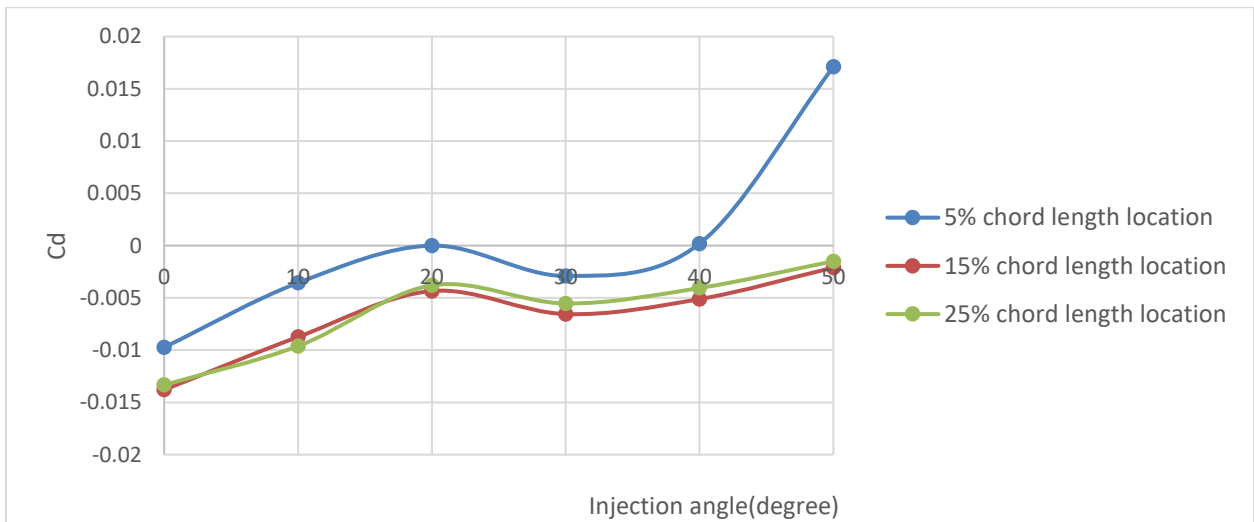


Figure 33: Drag coefficients variation with injection angle; $C_{\mu} = 0.1$, $\alpha = 10^{\circ}$.

6.2 Sharp change in aerodynamic coefficient for a combination of C_{μ} , injection slot location and high injection angle

From section 6.1, it can be noted that there is a sharp change in aerodynamic coefficients when injection slot is located at 5% chord length location, $C_{\mu} = 0.1$, $\alpha = 10^{\circ}$ and injection angle is 50° . However, when injection slot is located at 15% or 25% chord length location, there is no sharp change in aerodynamic coefficients. To explain this phenomenon more clearly, the influence of injection angle from 0° to 60° is studied for various locations of the injection slot when $C_{\mu} = 0.1$. The results are shown in Figure 34 and 35. When the injection angle becomes 60° , there is sharp change in C_l and C_d when injection slot is at 5% chord length location and there is no sharp change when injection slot is located at 15% or 25% injection location.

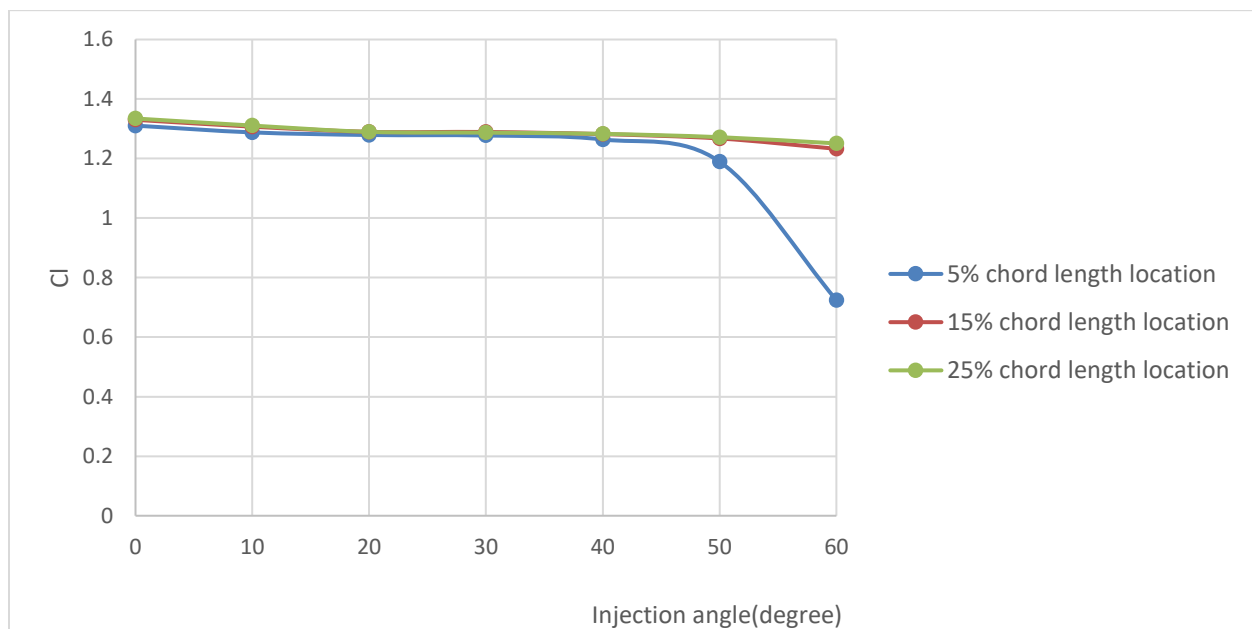


Figure 34: Lift coefficients variation with injection angle; $C_{\mu} = 0.1$, $\alpha = 10^{\circ}$.

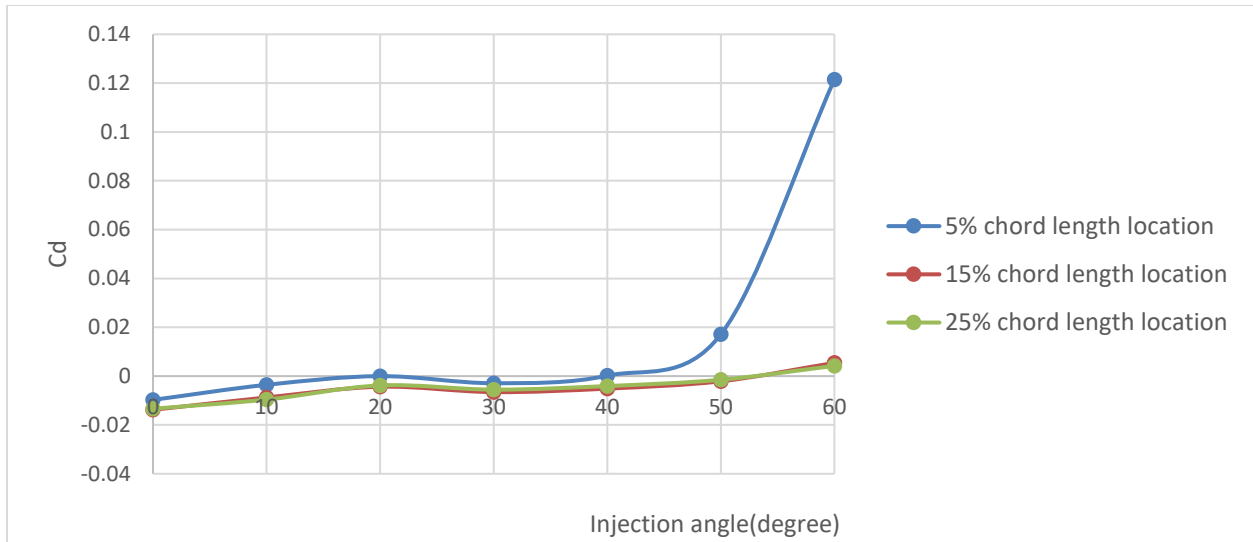
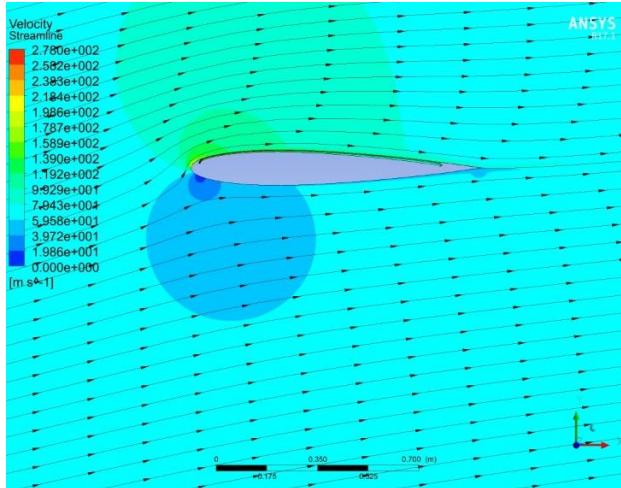


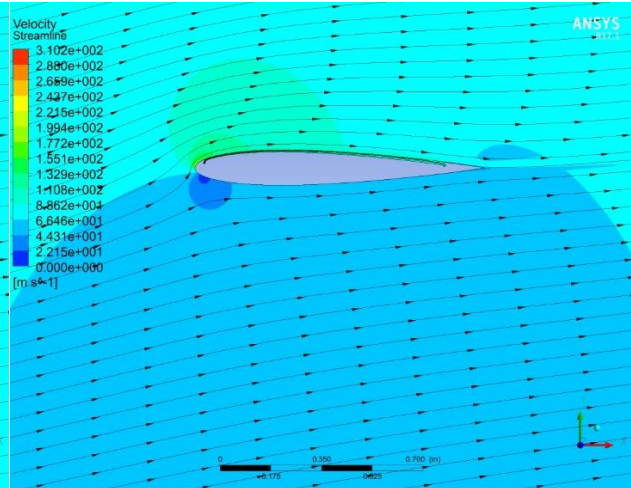
Figure 35: Drag coefficients variation with injection angle; $C_{\mu} = 0.1$, $\alpha = 10^{\circ}$.

Figure 36 shows the streamlines and velocity vectors around the NACA0012 airfoil in different injection angles when $C_{\mu} = 0.1$, $\alpha = 10^{\circ}$ and injection slot is at 5% chord length location. Figure 37 shows the streamlines and vectors around the NACA0012 airfoil at different injection angles when $C_{\mu} = 0.1$, $\alpha = 10^{\circ}$ and injection slot is at 15% chord length location. It shows that when injection slot is located at 5% chord length location, the flow separation occurs when injection angle is 60° .

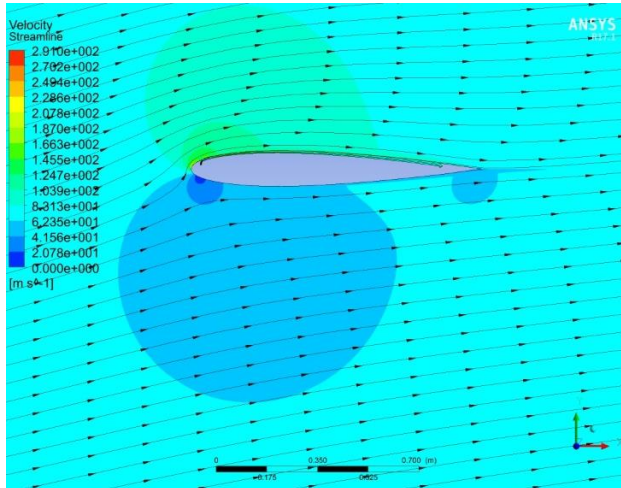
Figures 38-40 show the streamlines and velocity vectors near the injection slots when injection angles are all 60° . It shows that when injection slot is at 15% or 25% chord length location, there is no obvious flow separation like the one observed when injection slot is at 5% chord length location.



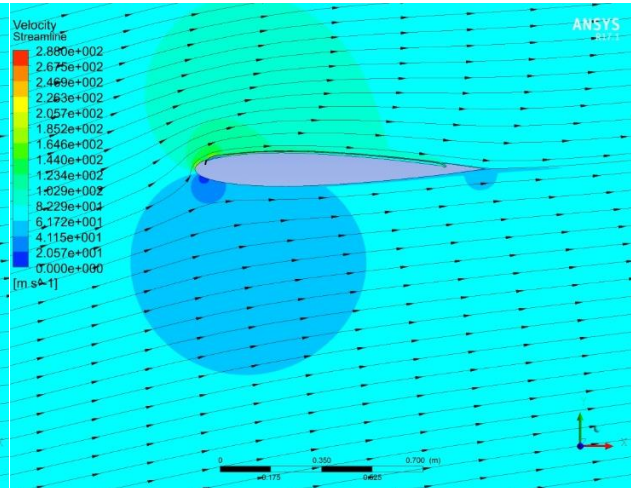
injection angle = 10°



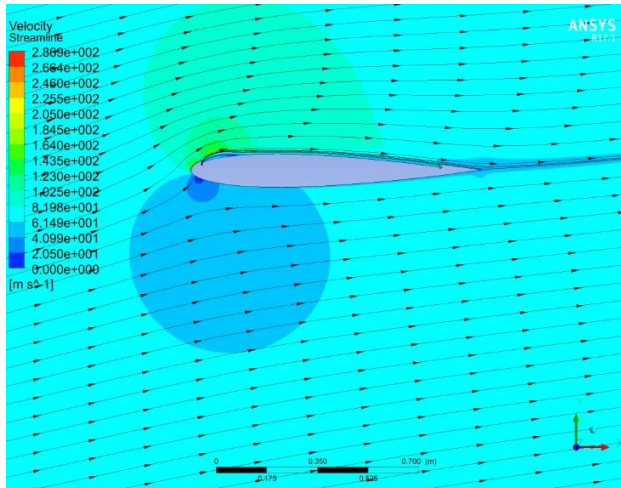
injection angle = 20°



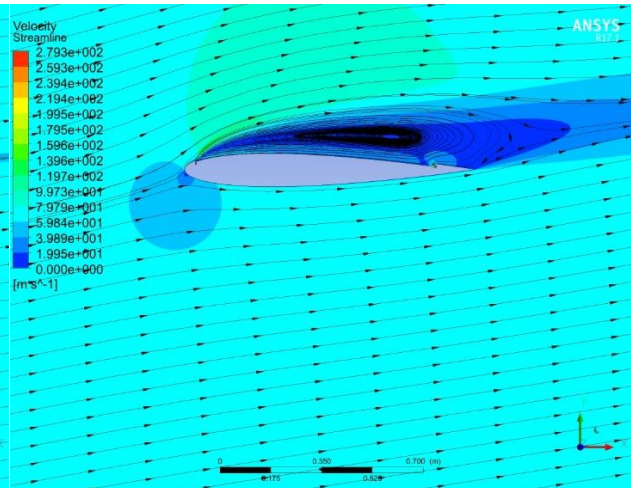
injection angle = 30°



injection angle = 40°

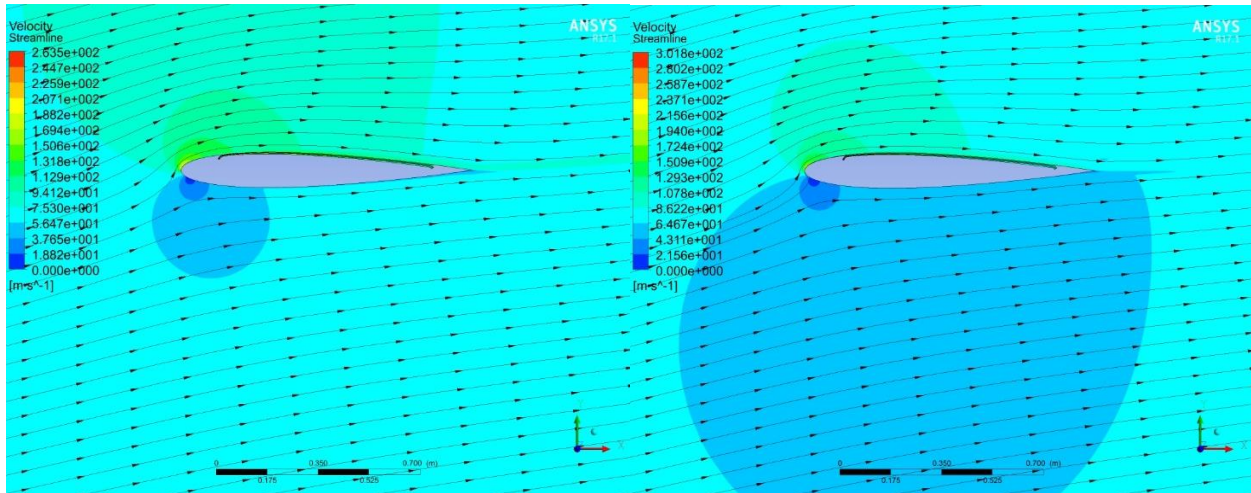


injection angle = 50°



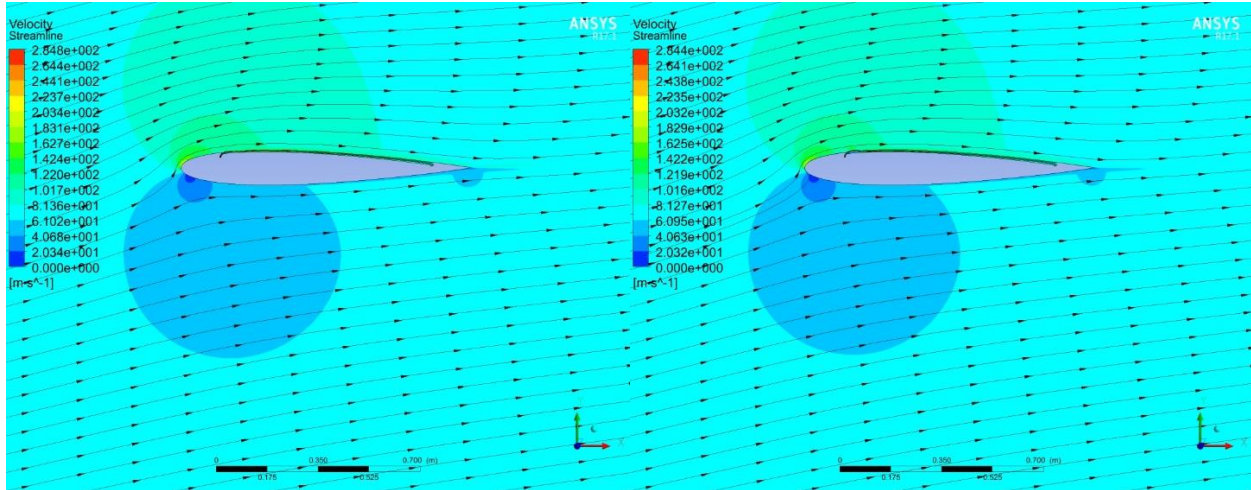
injection angle = 60°

Figure 36: Streamlines and velocity vectors for 10° to 60° injection angles at 5% chord length location when $C_{\mu} = 0.1$ and $\alpha = 10^\circ$.



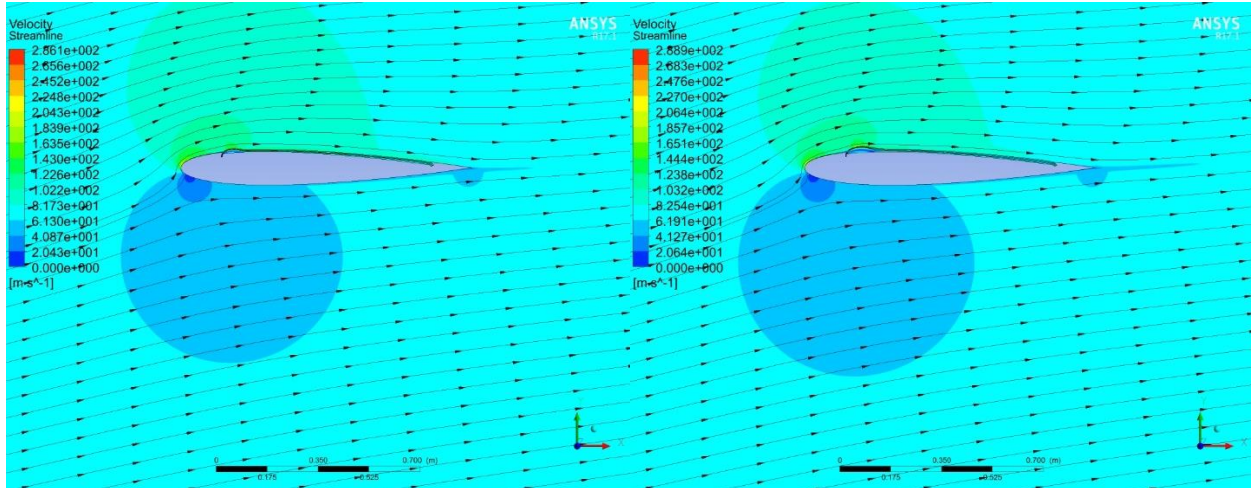
injection angle = 10°

injection angle = 20°



injection angle = 30°

injection angle = 40°



injection angle = 50°

injection angle = 60°

Figure 37: Streamlines and velocity vectors for 10° to 60° injection angles at 15% chord length location when $C_{\mu} = 0.1$ and $\alpha = 10^\circ$.

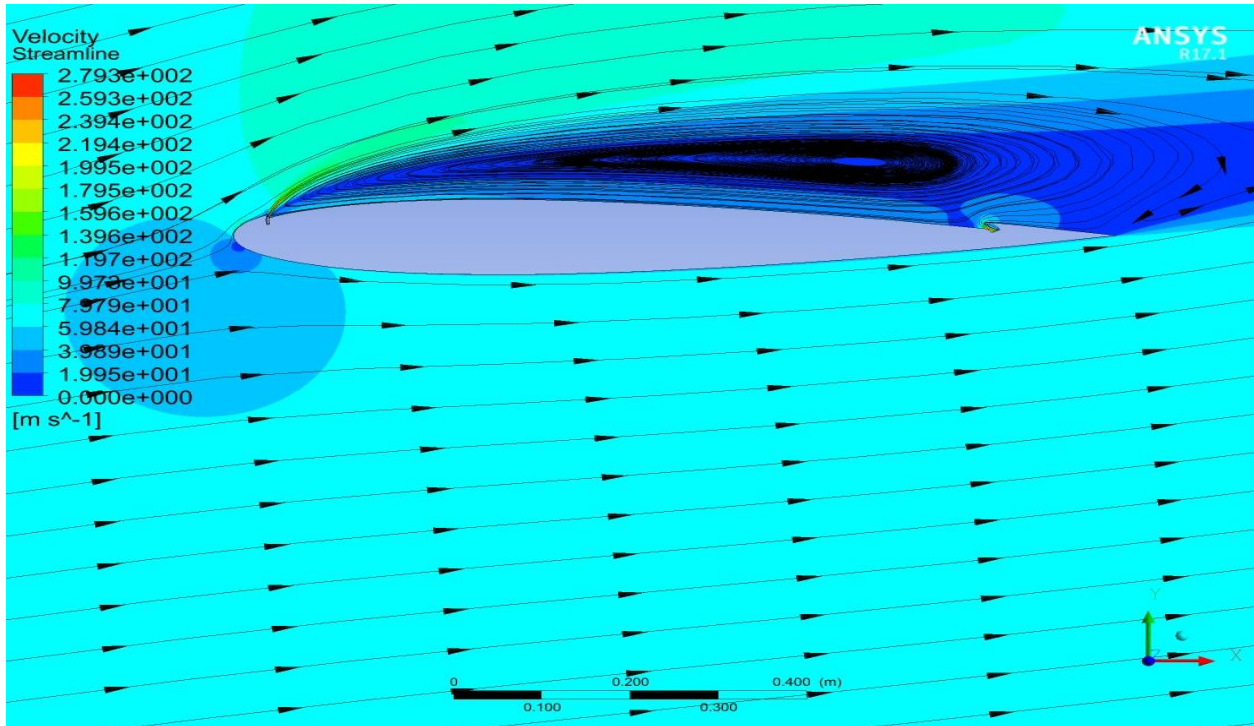


Figure 38: Streamlines and velocity vectors for 60° injection angles at 5% chord length location when $C_\mu = 0.1$ and $\alpha = 10^\circ$.

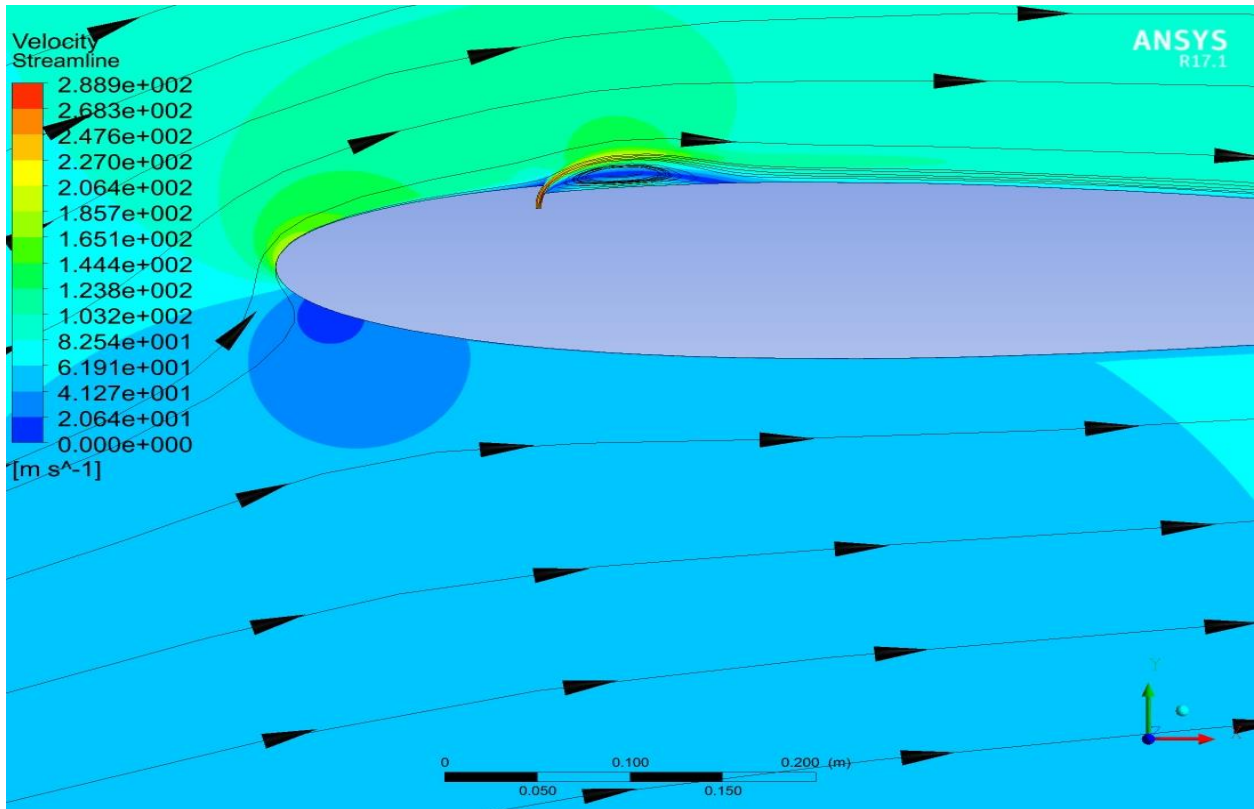


Figure 39: Streamlines and velocity vectors for 60° injection angles at 15% chord length location when $C_\mu = 0.1$ and $\alpha = 10^\circ$.

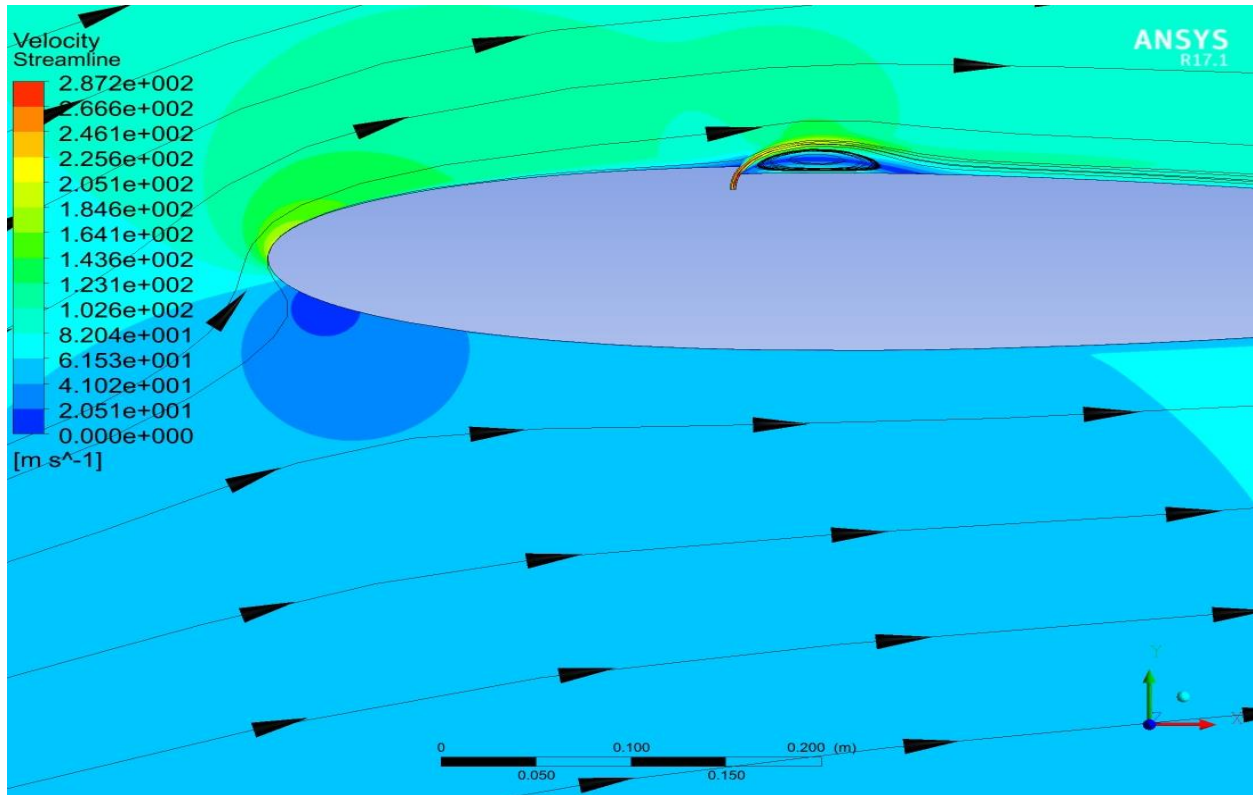


Figure 40: Streamlines and velocity vectors for 60° injection angles at 25% chord length location when $C_\mu = 0.1$ and $\alpha = 10^\circ$.

To define a best injection slot location to increase the stall margin, there are different aspects that need to be considered. First, when injection slot location is at 5% chord length location, it has relatively smaller injection angle range without the sharp change in C_l and C_d , 0° to 40° . When injection slot location is at 15% or 25%, the injection angle range is at least from 0° to 60° without sudden change in C_l and C_d . Second, from the results in section 6.1, when injection slot location is at 5% or 15% chord length location, the NACA0012 airfoil has relatively larger changes in absolute lift coefficient and in the relative lift coefficient compared to when injection slot location is at 25% chord length location. When injection slot location is at 5% or 15% chord length location and $C_\mu = 0.3$, the NACA0012 airfoil has relatively larger lift coefficients at all different injection angles compared to when injection slot location is at 25% chord length location and $C_\mu = 0.3$. When injection slot location is at 15% chord length location and $C_\mu = 0.2$

or 0.1, the NACA0012 airfoil has the largest lift coefficients for most injection angles. Third, for most of the cases in Table 1, when injection slot location is at 15% chord length, the drag coefficients are the smallest.

Thus, after considering sharp changes in C_l and C_d in both the relative and absolute lift coefficients for large injection angles, 15% chord length location appears to be the best injection slot location for changeable injection angles technology for CFJ.

6.3 Injection angle’s influence on stall angle

As shown in Table 2, nine different cases are studied to find the influence of injection angle on stall angle. Because the largest injection angle that does not cause sharp change when injection slot is at 5% chord length is 40° . 40° is chosen in B5 to B8 to study the influence on stall angle of the injection angle. In this section, flow past CFJ NACA0012 airfoil with changeable injection angle is compared to the flow past a traditional tangential CFJ NACA0012 airfoil. From results in section 6.1 and section 6.2, when the injection slot is at 25% chord length location, the airfoil has worst results for aerodynamic coefficients, thus 25% chord length location is not studied in this section.

Cases	C_μ	Injection angle	Injection slot location	AoA
B1	0.1	0°	5%	Around the stall angle
B2	0.2	0°	5%	
B3	0.1	0°	15%	
B4	0.2	0°	15%	
B5	0.1	40°	5%	
B6	0.2	40°	5%	
B7	0.1	40°	15%	
B8	0.2	40°	15%	
B9(original airfoil)	N/A	N/A	N/A	

Table 2: Geometry parameters for stall angle analysis.

Figure 41 shows the results of cases B1, B2 and B9 and Figure 42 shows the results of cases B5, B6 and B9. Figures 41 and 42 show the aerodynamic coefficients for different angle of attack when injection slot is at 5% chord length location.

From Zha et al.'s papers [5-7], it can be noted for a thick airfoil like NACA0025, the tangential CFJ control can increase the stall angle significantly. However, NACA0012 airfoil is a thin airfoil and thus the increase in stall angle of tangential CFJ control is not significant. Figure 41 shows that the original NACA0012 airfoil has stall angle of 17° and tangential CFJ NACA0012 airfoil has stall angle at 20° when C_{μ} is 0.1 or 0.2.

Figure 42 shows the results when the injection angle becomes 40° . This figure shows that, when the injection slot is at 5% chord length location, there is a significant decrease in stall angle if injection angle becomes larger. When C_{μ} is 0.1 and injection angle is 40° , the stall angle becomes 14° . When C_{μ} is 0.2 and injection angle is 40° , the stall angle becomes 17° .

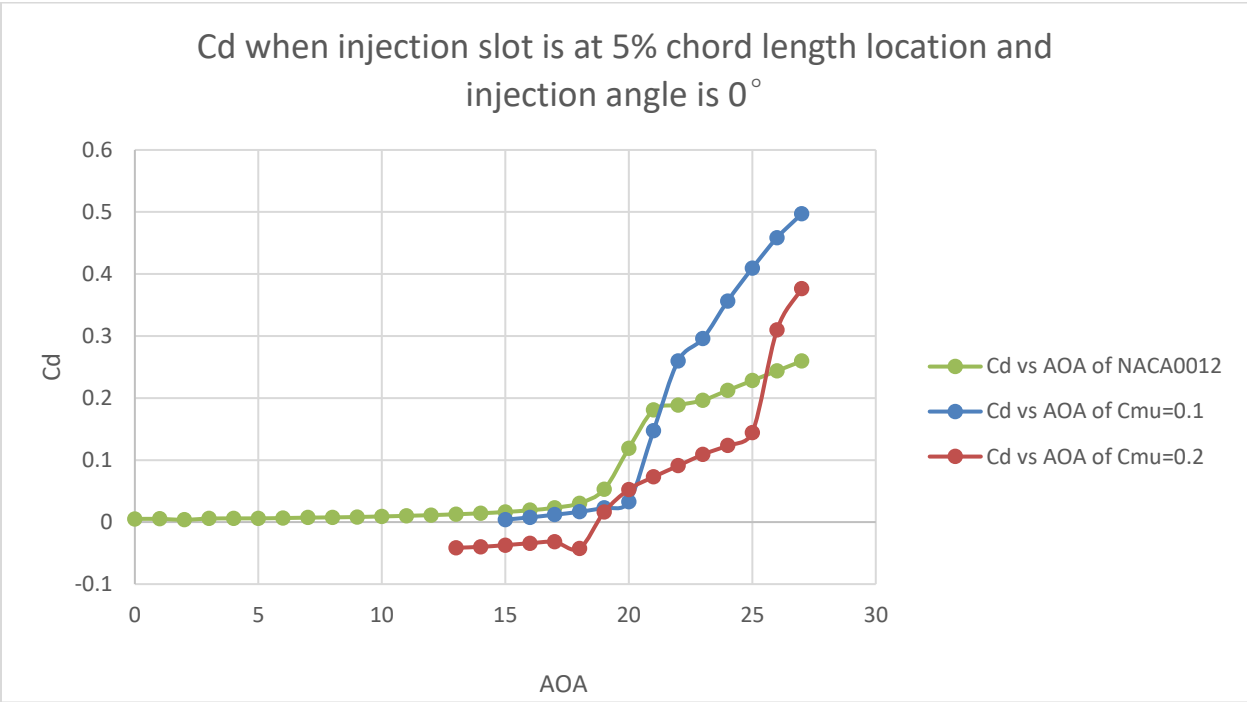
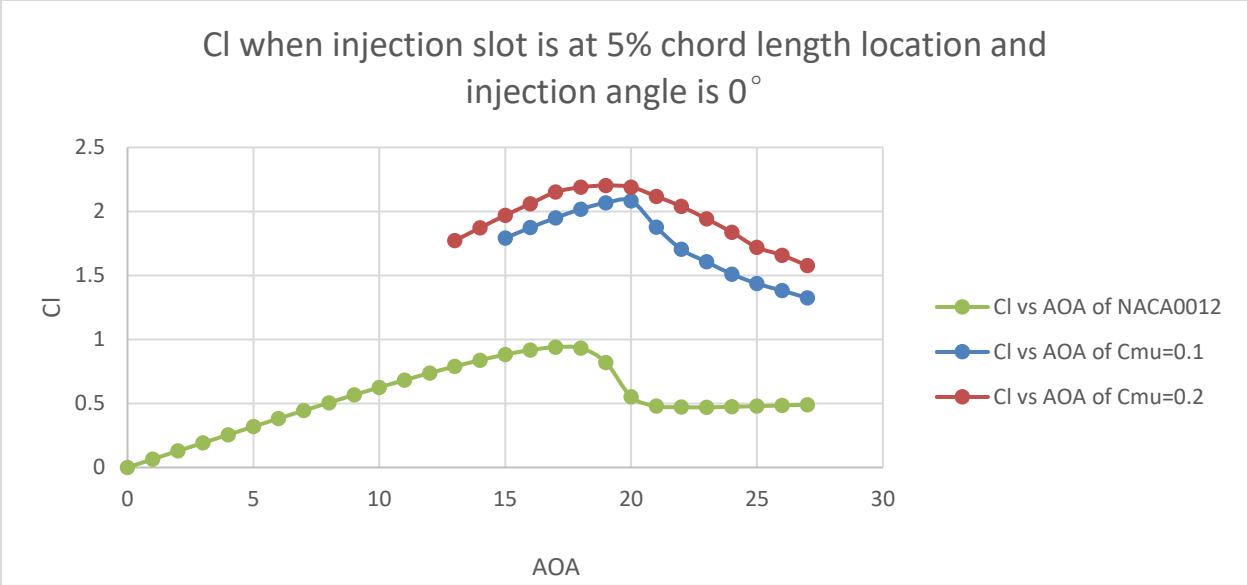


Figure 41: Stall angle analysis when injection slot is at 5% chord length location and injection angle is 0°.

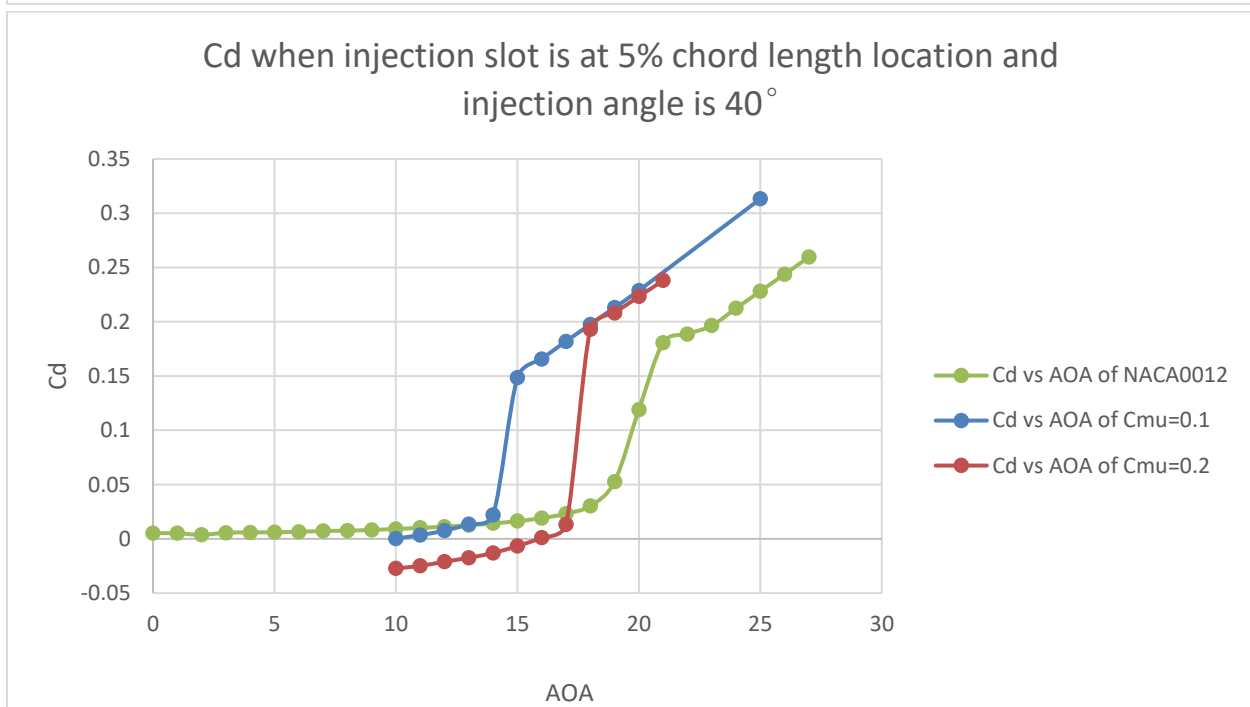
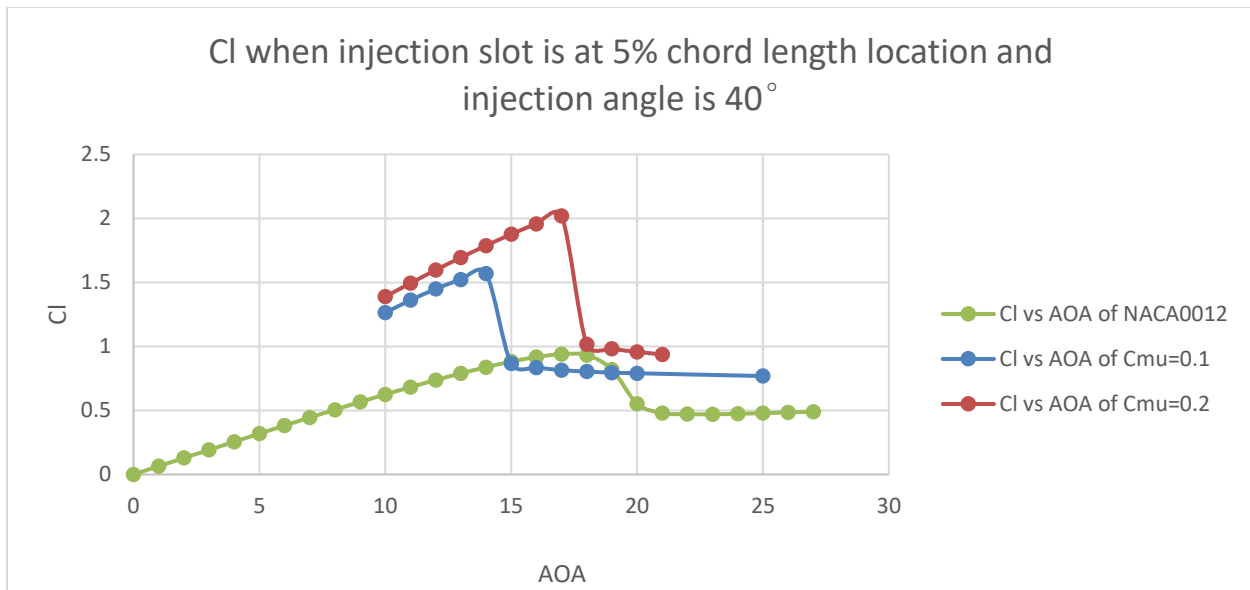


Figure 42: Stall angle analysis when injection slot is at 5% chord length location and injection angle is 40°.

Figure 43 shows the results of B3, B4 and B9 and Figure 44 shows the results of B7, B8 and B9. Figures 43 and 44 show the aerodynamic coefficients at different angle of attack when injection slot is at 15% chord length location.

Figure 43 shows that the increase in stall angle caused by tangential CFJ NACA0012 airfoil is still small when injection slot is at 15% chord length location. When $C_{\mu} = 0.1$, the stall angle is 19° and when $C_{\mu} = 0.2$, the stall angle is 18° . Figure 44 shows the results when injection angle becomes 40° and injection slot is at 15% chord length location. It shows that the stall angle is 20° when $C_{\mu} = 0.1$ and stall angle is 18° when $C_{\mu}=0.2$. Thus, when injection slot is at 15% chord length location, the change in stall angle caused by changeable injection angle is very small.

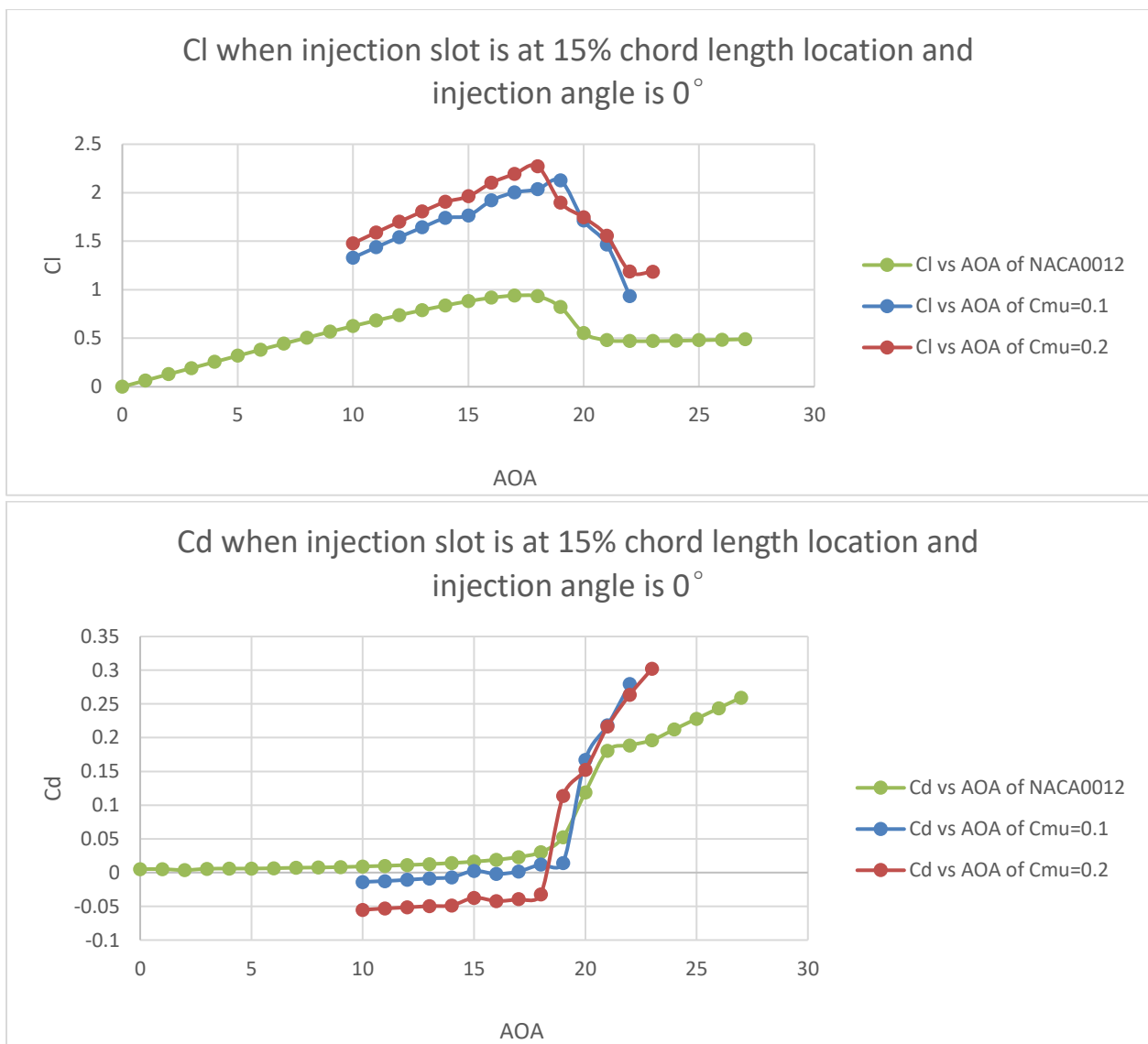


Figure 43: Stall angle analysis when injection slot is at 15% chord length location and injection angle is 0° .

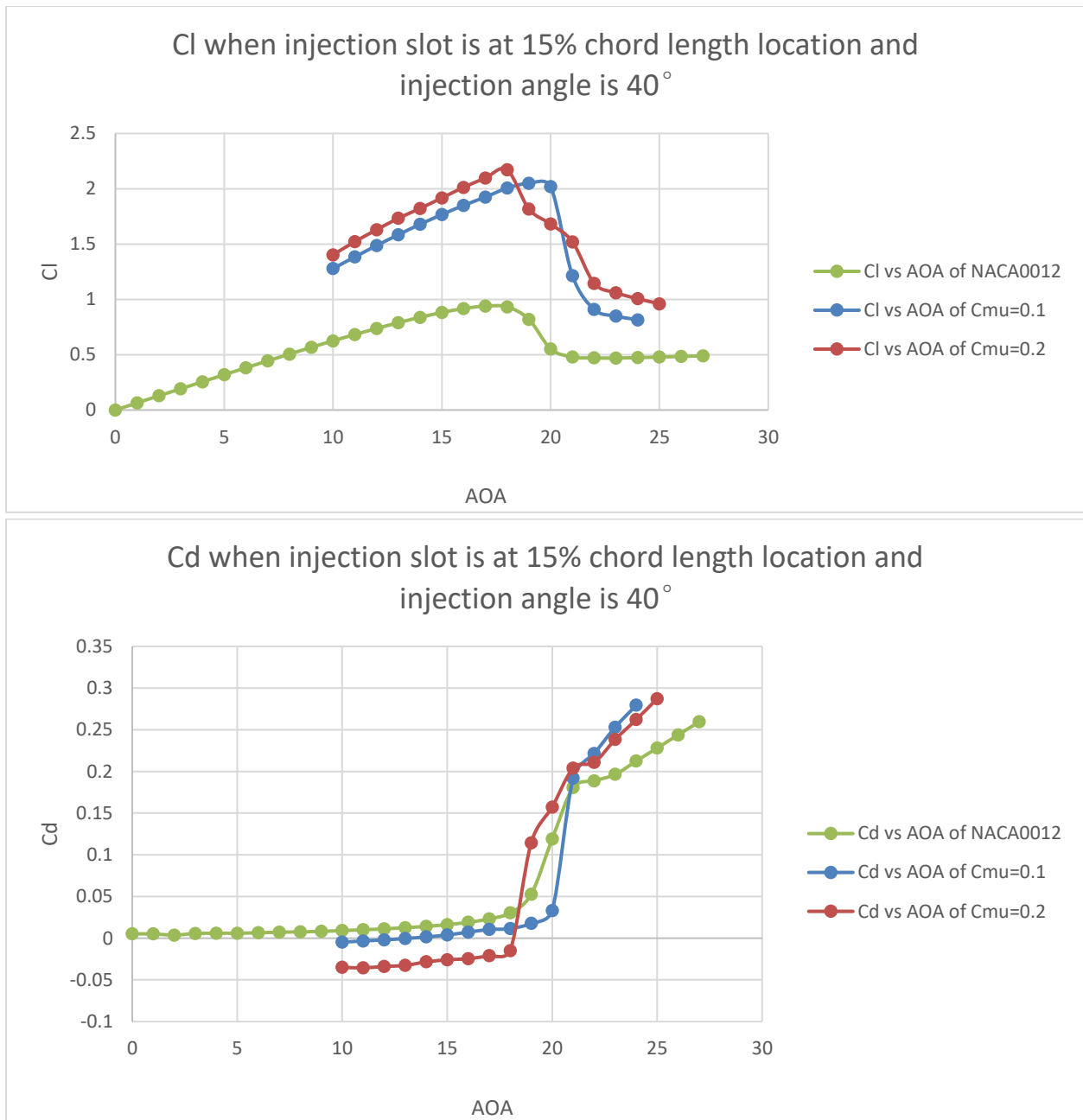


Figure 44: Stall angle analysis when injection slot is at 15% chord length location and injection angle is 40°.

It can be concluded that, when injection angle is changed from 0° to 40°, if injection slot is at 5% chord length location, there will be a significant decrease in stall angle and the stall angle will become smaller than the stall angle of original NACA0012 airfoil. When injection angle is changed from 0° to 40°, if injection slot is at 15% chord length location, there will be very small

change in the stall angle and the stall angle is nearly the same as the stall angle of original NACA0012 airfoil.

Thus, 15% chord length location is the best location for injection slot to implement the changeable injection angle technology with CFJ for controlling the lift and drag of an airfoil.

Chapter 7: Conclusions

This thesis has studied the influence on aerodynamic coefficients of NACA0012 airfoil when changeable injection angle CFJ control technology is employed to modulate its lift and drag coefficient. By comparing the aerodynamic performance of changeable injection angle CFJ control method with tangential CFJ control method, a best injection slot location is found from the three different locations considered that can employ the changeable injection angle CFJ technology to change the aerodynamic coefficients significantly but having little influence on stall angle. The main conclusions can be summarized as the follows:

- 1) Changeable injection angle CFJ technology can be employed to control the aerodynamic coefficients of an airfoil. When the injection angle becomes larger, the lift coefficient becomes smaller and drag coefficient becomes larger.
- 2) Changeable injection angle CFJ control method has influence on stall angle of an airfoil. When injection angle becomes larger, the stall angle becomes smaller.
- 3) For different injection slot locations, the influence of changeable injection angle CFJ control method on aerodynamic coefficients and stall angle is very different. After comparing the aerodynamic coefficients at three different locations of injection slot on the airfoil with various $C_{\mu} = 0.1, 0.2$ and 0.3 , and AoA of 0° and 10° , it was found that when injection slot is at 15% chord length location, the NACA0012 airfoil always has relatively larger lift coefficient and smaller drag coefficient and has larger relative changes in lift coefficients for most of the cases.
- 4) When C_{μ} becomes larger and AoA becomes smaller, the relative changes in lift coefficients become larger for all injection angles. When C_{μ} is 0.3 and AoA is 0° and

injection slot is at 15% chord length location (Figure 12), changeable injection angle CFJ technology has largest relative changes in lift coefficients for all injection angles. When injection angle becomes 50° , the relative change in lift coefficient can be 35%.

- 5) When injection slot location is at 5% chord length location, there is a sharp change in aerodynamic coefficients when injection angle becomes 40° . When injection slot location is at 15% or 25% chord length location, there is no sharp change in aerodynamic coefficients when injection angle changes from 0° to 60° .
- 6) When injection slot is at 5% chord length location, there is significant decrease in stall angle when injection angle changes from 0° to 40° . When injection slot is at 15% chord length location, there is nearly no change in stall angle when injection angle changes from 0° to 40° .

Thus, it can be concluded that the changeable injection angle CFJ technology can control the aerodynamic coefficients and the best injection slot location to employ this technology is at 15% chord length location for NACA0012 airfoil. The changeable injection angle method can be effectively used by appropriately changing the C_μ to control the aerodynamic coefficients of the airfoil in an effective way to achieve a desired outcome.

References

- [1]. Lefebvre, A. and Zha, G.-C., "Design of High Wing Loading Compact Electric Airplane Utilizing Co-Flow Jet Flow Control," AIAA Paper 2015-0772, AIAA SciTech2015: 53rd Aerospace Sciences Meeting, Kissimmee, FL, 5-9 Jan 2015.
- [2]. Zha, G.-C., Paxton, C., Conley, A., Wells, A., and Carroll, B., "Effect of Injection Slot Size on High Performance Co-Flow Jet Airfoil," *Journal of Aircraft*, Vol. 43, No. 4, July-Aug. 2006, pp. 987–995.
- [3]. Dano, B. P. E., Kirk, D., and Zha, G.-C., "Experimental Investigation of Jet Mixing Mechanism of Co- Flow Jet Airfoil," AIAA Paper 2010-4421, 5th AIAA Flow Control Conference, Chicago, IL, 28 Jun - 1 Jul 2010.
- [4]. Dano, B. P. E., Zha, G.-C., and Castillo, M., "Experimental Study of Co-Flow Jet Airfoil Performance Enhancement Using Micro Discret Jets," AIAA Paper 2011-0941, 49th AIAA Aerospace Sciences Meeting, Orlando, FL, 4-7 January 2011.
- [5]. Zha, G.-C., Carroll, B., Paxton, C., Conley, A., and Wells, A., "High Performance Airfoil with Co-Flow Jet Flow Control," AIAA Paper 2005-1260, 43rd AIAA Aerospace Sciences Meeting, Reno, NV, 10-13 January 2005.
- [6]. Zha, G.-C., Gao, W., and Paxton, D. C., "Jet Effects on Co-flow Jet Airfoil Performance," *AIAA Journal*, Vol. 45, No. 6, 2007, pp. 1222-1231.
- [7]. Zha, G.-C., and Paxton, D. C., "A Novel Flow Control Method for Airfoil Performance Enhancement Using Co-Flow Jet," *Progress in Astronautics and Aeronautics*, Chapter 10 - Applications of Circulation Control Technologies, Editors: Joslin, R. D. and Jones, G.S., Vol. 214, AIAA, Reston, VA, 2006, pp. 293-314.
- [8]. Wang, B.-Y. and Haddoukessouni, B. and Levy, J. and Zha, G.-C., "Numerical Investigations of Injection Slot Size Effect on the Performance of Co-Flow Jet Airfoil," *Journal of Aircraft*, Vol. 45, No. 6, 2008, pp.2084-2091.
- [9]. Lefebvre, A. and Dano, B. and Bartow, W. and Di Franzo, M. and Zha, G.-C., "Performance Enhancement and Energy Expenditure of Co-Flow Jet Airfoil with Variation of Mach number," AIAA Paper 2013-0490, *AIAA Journal of Aircraft*, DOI: 10.2514/1.C033113, 2016.
- [10]. Yang, Y., and Zha, G.-C., "Super-Lift Coefficient of Active Flow Control Airfoil: What is the Limit?" AIAA Paper 2017-1693, AIAA SciTech 2017, 55th AIAA Aerospace Science Meeting, Grapevine, TX, 9-13 January 2017.
- [11]. Liu, Z.-X., and Zha, G.-C., "Transonic Airfoil Performance Enhancement Using Co-Flow Jet Active Flow Control," AIAA Paper 2016-3066, AIAA Aviation, 13 -17 June 2016.

- [12]. Anders, S., Sellers, W. L., and Washburn, A., “Active Flow Control Activities at NASA Langley,” AIAA Paper 2004-2623, June 2004.
- [13]. Miller, D., and Addington, G., “Aerodynamic Flowfield Control Technologies for Highly Integrated Airframe Propulsion Flowpaths,” AIAA Paper 2004-2625, June 2004.
- [14]. Sellers, W. L. I., Singer, B. A., and Leavitt, L. D., “Aerodynamics for Revolutionary Air Vehicles,” AIAA Paper 2004-3785, June 2003.
- [15]. Kibens, V., and Bower, W. W., “An Overview of Active Flow Control Applications at the Boeing Company,” AIAA Paper 2004-2624, June 2004.
- [16]. Tilmann, C. P., Kimmel, R. L., Addington, G., and Myatt, J. H., “Flow Control Research and Application at the AFRL’s Air Vehicles Directorate,” AIAA Paper 2004-2622, June 2004.
- [17]. Gad-el Hak, M., Flow Control, Passive, Active, and Reactive Flow Management, Cambridge Univ. Press, Cambridge, England, 2000.
- [18]. Gad-el Hak, M., “Flow Control: The Future,” Journal of Aircraft, Vol. 38, No. 3, 2001, pp. 402–418.
- [19]. Gregory, Nigel, and C. L. O’reilly, “Low-Speed Aerodynamic Characteristics of NACA 0012 Airfoil Section Including the Effects of Upper-Surface Roughness Simulating Hoar Frost,” HM Stationery Office, London, 1973.

Appendix

UDF for C_μ

```
#include "udf.h"
```

```
#include "math.h"
```

```
#define FARLET_INDEX 82
```

```
#define INLET_INDEX 13
```

```
#define OUTLET_INDEX 14
```

```
#define INTERFACE_INDEX 38
```

```
#define S 1
```

```
#define injection_size 0.005
```

```
#define tarvalue_Cmu 0.1
```

```
static float flow_inlet;
```

```
static float flow_outlet;
```

```
static float pressure_inlet_0;
```

```
static float pressure_inlet_1;
```

```
static float pre_pressure_inlet_1;
```

```
static float change_pressure_inlet_1;
```

```
static float pressure_outlet_0;
```

```
static float pressure_outlet_1;
```

```
static float calvalue_Cmu;
```

```
static float pre_Cmu;
```

```
static float change_Cmu;
```

```
static float pre_flow_outlet;
```

```
static float change_flow_outlet;
```

```

Domain *domain;

Thread *thread_inlet;

Thread *thread_outlet;

Thread *thread_farlet;

Thread *thread_interface;

void calculate_Cmu(Thread *thread_farlet, Thread *thread_outlet, Thread *thread_inlet,
Thread *thread_interface)

{
/* velocity from interface, divided by density and injectionsize, with cell loop, both
density and pressure based, for parallel*/

    cell_t c;
    cell_t c0;
    cell_t c1;
    face_t f;
    Thread *t0;
    Thread *t1;
    int i = 0;
    float velocity[2];
    float velocity_farlet = 0.0;
    float velocity_inlet = 0.0;
    float local_velocity_inlet = 0.0;
    float density_farlet = 0.0;
    float density_inlet = 0.0;
    float density_interface = 0.0;
    flow_inlet = 0.0;
    flow_outlet = 0.0;
    pressure_inlet_0 = 0.0;
    pressure_outlet_0 = 0.0;

```

```

#if !RP_HOST
    begin_f_loop(f, thread_farlet)
    {
        if (PRINCIPAL_FACE_P(f,thread_farlet))
        {
            c0 = F_C0(f, thread_farlet);
            t0 = F_C0_THREAD(f, thread_farlet);
            density_farlet += C_R(c0, t0);
            velocity[0] = C_U(c0, t0);
            velocity[1] = C_V(c0, t0);
            velocity_farlet += NV_MAG(velocity);
            i++;
        }
    }
    end_f_loop(f, thread_farlet)

    # if RP_NODE
        density_farlet = PRF_GRSUM1(density_farlet);
        velocity_farlet = PRF_GRSUM1(velocity_farlet);
        i = PRF_GRSUM1(i);
    # endif
#endif

node_to_host_float_2(density_farlet, velocity_farlet);
node_to_host_int_1(i);

#if !RP_NODE

```

```

density_farlet = density_farlet/i;
velocity_farlet = velocity_farlet/i;
    Message("moniter density_farlet = %f\n", density_farlet);
#endif

#if !RP_HOST
    i = 0;

    begin_f_loop(f, thread_outlet)
    {
        if (PRINCIPAL_FACE_P(f,thread_outlet))
        {
            flow_outlet += F_FLUX(f, thread_outlet);
            pressure_outlet_0 += F_P(f, thread_outlet);
            i++;
        }
    }
    end_f_loop(f, thread_outlet)

    # if RP_NODE
        flow_outlet = PRF_GRSUM1(flow_outlet);
        pressure_outlet_0 = PRF_GRSUM1(pressure_outlet_0);
        i = PRF_GRSUM1(i);
    # endif
#endif

node_to_host_float_2(flow_outlet, pressure_outlet_0);
node_to_host_int_1(i);

```

```

#if !RP_NODE
    pressure_outlet_0 = pressure_outlet_0/i;
#endif

#if !RP_HOST
    i = 0;

    begin_f_loop(f, thread_inlet)
    {
        if (PRINCIPAL_FACE_P(f,thread_inlet))
        {
            flow_inlet += F_FLUX(f, thread_inlet);
            pressure_inlet_0 += F_P(f, thread_inlet);
            i++;
        }
    }
    end_f_loop(f, thread_inlet)

    # if RP_NODE
        flow_inlet = PRF_GRSUM1(flow_inlet);
        pressure_inlet_0 = PRF_GRSUM1(pressure_inlet_0);
        i = PRF_GRSUM1(i);
    # endif
#endif

node_to_host_float_2(flow_inlet, pressure_inlet_0);
node_to_host_int_1(i);

```

```

#if !RP_NODE
    pressure_inlet_0 = pressure_inlet_0/i;
#endif

#if !RP_HOST
    i = 0;

    begin_f_loop(f, thread_inlet)
    {
        if (PRINCIPAL_FACE_P(f,thread_inlet))
        {
            c0 = F_C0(f, thread_inlet);
            t0 = F_C0_THREAD(f, thread_inlet);
            density_inlet += C_R(c0, t0);
            i++;
        }
    }
    end_f_loop(f, thread_inlet)

    # if RP_NODE
        density_inlet = PRF_GRSUM1(density_inlet);
        i = PRF_GRSUM1(i);
    # endif
#endif

node_to_host_float_1(density_inlet);
node_to_host_int_1(i);

```

```

#if !RP_NODE

    density_inlet = density_inlet/i;

    Message("moniter density_inlet = %f\n", density_inlet);

    local_velocity_inlet = flow_inlet/density_inlet/injectionsize;

#endif

#if !RP_HOST

    i = 0;

    begin_f_loop(f, thread_interface)
    {
        if (PRINCIPAL_FACE_P(f,thread_interface))
        {
            c0 = F_C0(f, thread_interface);
            c1 = F_C1(f, thread_interface);
            t0 = F_C0_THREAD(f, thread_interface);
            t1 = F_C1_THREAD(f, thread_interface);

            density_interface += (C_R(c0, t0)+C_R(c1, t1))/2.0;

            i++;
        }
    }
    end_f_loop(f, thread_interface)

    # if RP_NODE

        density_interface = PRF_GRSUM1(density_interface);

        i = PRF_GRSUM1(i);

```

```

        # endif
#endif

node_to_host_float_1(density_interface);
node_to_host_int_1(i);

#if !RP_NODE

    density_interface = density_interface/i;
    Message("moniter density_interface = %f\n", density_interface);
    velocity_inlet = flow_inlet/density_interface/injectionsize;

    velocity_inlet = fabs(velocity_inlet);
    Message("moniter velocity_inlet(interface) = %f\n", velocity_inlet);

    if(density_inlet* velocity_inlet != 0.0)
    {
        pressure_inlet_0 = pressure_inlet_0+ 1/ 2.0* density_inlet*
local_velocity_inlet* local_velocity_inlet;
    }
    Message("moniter pressure_inlet = %f\n", pressure_inlet_0);
    Message("moniter pressure_outlet = %f\n", pressure_outlet_0);

    if(density_farlet* velocity_farlet != 0.0)
    {
        calvalue_Cmu = flow_inlet* velocity_inlet/ (1/ 2.0* density_farlet*
velocity_farlet* velocity_farlet* S);
    }
    calvalue_Cmu = fabs(calvalue_Cmu);
    change_Cmu = calvalue_Cmu-pre_Cmu;

```



```

    pre_Cmu = calvalue_Cmu;

    change_flow_outlet = flow_outlet-pre_flow_outlet;

    pre_flow_outlet = flow_outlet;

#endif

}

DEFINE_INIT(Initialize_variable,domain)
{
/*349265*/

    calvalue_Cmu = tarvalue_Cmu;

    pre_pressure_inlet_1 = 0;
    change_pressure_inlet_1 = 0;

    pre_Cmu = 0;

    change_Cmu = 0;

    pre_flow_outlet = 0;

    change_flow_outlet = 0;

    pressure_inlet_1 = 100000;

    pressure_outlet_1 = -10000;

#if !RP_NODE

    Message("calvalue_Cmu = %f\t", calvalue_Cmu);

    Message("flow_inlet = %f\t", flow_inlet);

    Message("flow_outlet = %f\n", flow_outlet);

#endif

}

DEFINE_EXECUTE_AT_END(Set_EachIterate_masstwopercentchange)
{

    domain = Get_Domain(1);

```

```

thread_inlet = Lookup_Thread(domain, INLET_INDEX);

thread_outlet = Lookup_Thread(domain, OUTLET_INDEX);

thread_farlet = Lookup_Thread(domain, FARLET_INDEX);

thread_interface = Lookup_Thread(domain, INTERFACE_INDEX);

calculate_Cmu(thread_farlet, thread_outlet, thread_inlet, thread_interface);

#if !RP_NODE

    if(fabs(change_Cmu)<0.0005 & pressure_inlet_1<=400000&pressure_inlet_1>0)
    {
        if(calvalue_Cmu < tarvalue_Cmu* 0.999 & change_Cmu>=-0.001)
            pressure_inlet_1 += 10000*fabs(calvalue_Cmu - tarvalue_Cmu)*fabs(calvalue_Cmu - tarvalue_Cmu)+5000*fabs(calvalue_Cmu - tarvalue_Cmu);
            if(calvalue_Cmu > tarvalue_Cmu* 1.001 & change_Cmu<= 0.001)
                pressure_inlet_1 -= 10000*fabs(calvalue_Cmu - tarvalue_Cmu)*fabs(calvalue_Cmu - tarvalue_Cmu)+5000*fabs(calvalue_Cmu - tarvalue_Cmu);
    }

    if(pressure_inlet_1>400000)
    {
        pressure_inlet_1 = 400000;
    }

    change_pressure_inlet_1 = pressure_inlet_1-pre_pressure_inlet_1;
    pre_pressure_inlet_1 = pressure_inlet_1;

    flow_inlet = fabs(flow_inlet);
    Message("flow_inlet = %f\t", flow_inlet);

```

```

flow_inlet = 1.02*fabs(flow_inlet);

flow_outlet = flow_outlet;

Message("flow_outlet = %f\t", flow_outlet);

    if(fabs(change_Cmu)<0.001      &      change_pressure_inlet_1==0      &
fabs(change_flow_outlet)<0.01&fabs(flow_outlet- flow_inlet)<=0.1)
    {
        if(fabs(flow_outlet- flow_inlet) > (flow_inlet+ flow_outlet)/ 2.0* 0.0005
|| flow_outlet < flow_inlet)
        {
            if(flow_inlet > flow_outlet)
                pressure_outlet_1 -= fabs(flow_inlet- flow_outlet)*50+1;
            if(flow_inlet < flow_outlet)
                pressure_outlet_1 += fabs(flow_inlet- flow_outlet)*50+1;
        }
    }

    if(fabs(change_Cmu)<0.001 & change_pressure_inlet_1==0 & fabs(flow_outlet-
flow_inlet)>0.1)
    {
        if(fabs(flow_outlet- flow_inlet) > (flow_inlet+ flow_outlet)/ 2.0* 0.0005
|| flow_outlet < flow_inlet)
        {
            if(flow_inlet > flow_outlet)
                pressure_outlet_1 -= fabs(flow_inlet- flow_outlet)*50+1;
            if(flow_inlet < flow_outlet)
                pressure_outlet_1 += fabs(flow_inlet- flow_outlet)*50+1;
        }
    }

    if(fabs(change_Cmu)<0.001 & change_pressure_inlet_1!=0)
    {

```

```

        if(fabs(flow_outlet- flow_inlet) > (flow_inlet+ flow_outlet)/ 2.0* 0.0005
|| flow_outlet < flow_inlet)
        {
            if(flow_inlet > flow_outlet)
                pressure_outlet_1 -= fabs(flow_inlet- flow_outlet)*50+1;
            if(flow_inlet < flow_outlet)
                pressure_outlet_1 += fabs(flow_inlet- flow_outlet)*50+1;
        }
    }
    Message("calvalue_Cmu = %f\t", calvalue_Cmu);
    Message("pressure_inlet = %f\t", pressure_inlet_1);
    Message("pressure_outlet = %f\n", pressure_outlet_1);
#endif

host_to_node_float_2(pressure_inlet_1, pressure_outlet_1);
}

DEFINE_EXECUTE_AT_END(Set_EachIterate_massonepercentchange)
{
    domain = Get_Domain(1);

    thread_inlet = Lookup_Thread(domain, INLET_INDEX);
    thread_outlet = Lookup_Thread(domain, OUTLET_INDEX);
    thread_farlet = Lookup_Thread(domain, FARLET_INDEX);
    thread_interface = Lookup_Thread(domain, INTERFACE_INDEX);

    calculate_Cmu(thread_farlet, thread_outlet, thread_inlet, thread_interface);
}

```

```

#if !RP_NODE

    if(fabs(change_Cmu)<0.0005 & pressure_inlet_1<=400000&pressure_inlet_1>0)
    {
        if(calvalue_Cmu < tarvalue_Cmu* 0.999 & change_Cmu>=-0.001)
            pressure_inlet_1 += 10000*fabs(calvalue_Cmu - tarvalue_Cmu)*fabs(calvalue_Cmu - tarvalue_Cmu)+5000*fabs(calvalue_Cmu - tarvalue_Cmu);
            if(calvalue_Cmu > tarvalue_Cmu* 1.001 & change_Cmu<= 0.001)
                pressure_inlet_1 -= 10000*fabs(calvalue_Cmu - tarvalue_Cmu)*fabs(calvalue_Cmu - tarvalue_Cmu)+5000*fabs(calvalue_Cmu - tarvalue_Cmu);
    }

    if(pressure_inlet_1>400000)
    {
        pressure_inlet_1 = 400000;
    }

    change_pressure_inlet_1 = pressure_inlet_1-pre_pressure_inlet_1;
    pre_pressure_inlet_1 = pressure_inlet_1;

    flow_inlet = fabs(flow_inlet);
    Message("flow_inlet = %f\t", flow_inlet);
    flow_inlet = 1.01*fabs(flow_inlet);
    flow_outlet = flow_outlet;
    Message("flow_outlet = %f\t", flow_outlet);

    if(fabs(change_Cmu)<0.001 & change_pressure_inlet_1==0 &
    fabs(change_flow_outlet)<0.01&fabs(flow_outlet- flow_inlet)<=0.1)
    {
        if(fabs(flow_outlet- flow_inlet) > (flow_inlet+ flow_outlet)/ 2.0* 0.0005
        || flow_outlet < flow_inlet)
        {

```

```

        if(flow_inlet > flow_outlet)
            pressure_outlet_1 -= fabs(flow_inlet- flow_outlet)*50+1;
        if(flow_inlet < flow_outlet)
            pressure_outlet_1 += fabs(flow_inlet- flow_outlet)*50+1;
    }
}
if(fabs(change_Cmu)<0.001 & change_pressure_inlet_1==0&fabs(flow_outlet-
flow_inlet)>0.1)
{
    if(fabs(flow_outlet- flow_inlet) > (flow_inlet+ flow_outlet)/ 2.0* 0.0005
|| flow_outlet < flow_inlet)
    {
        if(flow_inlet > flow_outlet)
            pressure_outlet_1 -= fabs(flow_inlet- flow_outlet)*50+1;
        if(flow_inlet < flow_outlet)
            pressure_outlet_1 += fabs(flow_inlet- flow_outlet)*50+1;
    }
}
if(fabs(change_Cmu)<0.001 & change_pressure_inlet_1!=0)
{
    if(fabs(flow_outlet- flow_inlet) > (flow_inlet+ flow_outlet)/ 2.0* 0.0005
|| flow_outlet < flow_inlet)
    {
        if(flow_inlet > flow_outlet)
            pressure_outlet_1 -= fabs(flow_inlet- flow_outlet)*50+1;
        if(flow_inlet < flow_outlet)
            pressure_outlet_1 += fabs(flow_inlet- flow_outlet)*50+1;
    }
}
Message("calvalue_Cmu = %f\t", calvalue_Cmu);

```

```

    Message("pressure_inlet = %f\t", pressure_inlet_1);
    Message("pressure_outlet = %f\n", pressure_outlet_1);
#endif

host_to_node_float_2(pressure_inlet_1, pressure_outlet_1);
}

DEFINE_EXECUTE_AT_END(Set_EachIterate_masshalfonepercentchange)
{
    domain = Get_Domain(1);

    thread_inlet = Lookup_Thread(domain, INLET_INDEX);
    thread_outlet = Lookup_Thread(domain, OUTLET_INDEX);
    thread_farlet = Lookup_Thread(domain, FARLET_INDEX);
    thread_interface = Lookup_Thread(domain, INTERFACE_INDEX);

    calculate_Cmu(thread_farlet, thread_outlet, thread_inlet, thread_interface);

#if !RP_NODE
    if(fabs(change_Cmu)<0.0005 & pressure_inlet_1<=400000&pressure_inlet_1>0)
    {
        if(calvalue_Cmu < tarvalue_Cmu* 0.999 & change_Cmu>=-0.001)
            pressure_inlet_1      +=      10000*fabs(calvalue_Cmu
tarvalue_Cmu)*fabs(calvalue_Cmu - tarvalue_Cmu)+5000*fabs(calvalue_Cmu - tarvalue_Cmu);
        if(calvalue_Cmu > tarvalue_Cmu* 1.001 & change_Cmu<= 0.001)
            pressure_inlet_1      -=      10000*fabs(calvalue_Cmu
tarvalue_Cmu)*fabs(calvalue_Cmu - tarvalue_Cmu)+5000*fabs(calvalue_Cmu - tarvalue_Cmu);
    }
#endif
}

```

```

if(pressure_inlet_1>400000)
{
    pressure_inlet_1 = 400000;
}

change_pressure_inlet_1 = pressure_inlet_1-pre_pressure_inlet_1;
pre_pressure_inlet_1 = pressure_inlet_1;

flow_inlet = fabs(flow_inlet);
Message("flow_inlet = %f\t", flow_inlet);
flow_inlet = 1.005*fabs(flow_inlet);
flow_outlet = flow_outlet;
Message("flow_outlet = %f\t", flow_outlet);

if(fabs(change_Cmu)<0.001 & change_pressure_inlet_1==0 &
fabs(change_flow_outlet)<0.01&fabs(flow_outlet- flow_inlet)<=0.1)
{
    if(fabs(flow_outlet- flow_inlet) > (flow_inlet+ flow_outlet)/ 2.0* 0.0005
|| flow_outlet < flow_inlet)
    {
        if(flow_inlet > flow_outlet)
            pressure_outlet_1 -= fabs(flow_inlet- flow_outlet)*50+1;
        if(flow_inlet < flow_outlet)
            pressure_outlet_1 += fabs(flow_inlet- flow_outlet)*50+1;
    }
}

if(fabs(change_Cmu)<0.001 & change_pressure_inlet_1==0&fabs(flow_outlet-
flow_inlet)>0.1)
{

```



```

        if(fabs(flow_outlet- flow_inlet) > (flow_inlet+ flow_outlet)/ 2.0* 0.0005
|| flow_outlet < flow_inlet)
        {
            if(flow_inlet > flow_outlet)
                pressure_outlet_1 -= fabs(flow_inlet- flow_outlet)*50+1;
            if(flow_inlet < flow_outlet)
                pressure_outlet_1 += fabs(flow_inlet- flow_outlet)*50+1;
        }
    }
    if(fabs(change_Cmu)<0.001 & change_pressure_inlet_1!=0)
    {
        if(fabs(flow_outlet- flow_inlet) > (flow_inlet+ flow_outlet)/ 2.0* 0.0005
|| flow_outlet < flow_inlet)
        {
            if(flow_inlet > flow_outlet)
                pressure_outlet_1 -= fabs(flow_inlet- flow_outlet)*50+1;
            if(flow_inlet < flow_outlet)
                pressure_outlet_1 += fabs(flow_inlet- flow_outlet)*50+1;
        }
    }
    Message("calvalue_Cmu = %f\t", calvalue_Cmu);
    Message("pressure_inlet = %f\t", pressure_inlet_1);
    Message("pressure_outlet = %f\n", pressure_outlet_1);
#endif

host_to_node_float_2(pressure_inlet_1, pressure_outlet_1);
}

DEFINE_EXECUTE_AT_END(Set_EachIterate)

```

```

{

domain = Get_Domain(1);

thread_inlet = Lookup_Thread(domain, INLET_INDEX);
thread_outlet = Lookup_Thread(domain, OUTLET_INDEX);
thread_farlet = Lookup_Thread(domain, FARLET_INDEX);
thread_interface = Lookup_Thread(domain, INTERFACE_INDEX);

calculate_Cmu(thread_farlet, thread_outlet, thread_inlet, thread_interface);

#if !RP_NODE

    if(fabs(change_Cmu)<0.0005 & pressure_inlet_1<=400000&pressure_inlet_1>0)
    {
        if(calvalue_Cmu < tarvalue_Cmu* 0.999 & change_Cmu>=-0.001)
            pressure_inlet_1 += 10000*fabs(calvalue_Cmu - tarvalue_Cmu)*fabs(calvalue_Cmu - tarvalue_Cmu)+5000*fabs(calvalue_Cmu - tarvalue_Cmu);
        if(calvalue_Cmu > tarvalue_Cmu* 1.001 & change_Cmu<= 0.001)
            pressure_inlet_1 -= 10000*fabs(calvalue_Cmu - tarvalue_Cmu)*fabs(calvalue_Cmu - tarvalue_Cmu)+5000*fabs(calvalue_Cmu - tarvalue_Cmu);
    }
    if(pressure_inlet_1>400000)
    {
        pressure_inlet_1 = 400000;
    }

    change_pressure_inlet_1 = pressure_inlet_1-pre_pressure_inlet_1;
    pre_pressure_inlet_1 = pressure_inlet_1;

```

```

flow_inlet = fabs(flow_inlet);

flow_outlet = flow_outlet;

    if(fabs(change_Cmu)<0.001      &      change_pressure_inlet_1==0      &
fabs(change_flow_outlet)<0.01&fabs(flow_outlet- flow_inlet)<=0.1)
    {
        if(fabs(flow_outlet- flow_inlet) > (flow_inlet+ flow_outlet)/ 2.0* 0.0005
|| flow_outlet < flow_inlet)
        {
            if(flow_inlet > flow_outlet)
                pressure_outlet_1 -= fabs(flow_inlet- flow_outlet)*50+1;
            if(flow_inlet < flow_outlet)
                pressure_outlet_1 += fabs(flow_inlet- flow_outlet)*50+1;
        }
    }

    if(fabs(change_Cmu)<0.001      &      change_pressure_inlet_1==0&fabs(flow_outlet-
flow_inlet)>0.1)
    {
        if(fabs(flow_outlet- flow_inlet) > (flow_inlet+ flow_outlet)/ 2.0* 0.0005
|| flow_outlet < flow_inlet)
        {
            if(flow_inlet > flow_outlet)
                pressure_outlet_1 -= fabs(flow_inlet- flow_outlet)*50+1;
            if(flow_inlet < flow_outlet)
                pressure_outlet_1 += fabs(flow_inlet- flow_outlet)*50+1;
        }
    }

    if(fabs(change_Cmu)<0.001 & change_pressure_inlet_1!=0)
    {

```

```

        if(fabs(flow_outlet- flow_inlet) > (flow_inlet+ flow_outlet)/ 2.0* 0.0005
|| flow_outlet < flow_inlet)
    {
        if(flow_inlet > flow_outlet)
            pressure_outlet_1 -= fabs(flow_inlet- flow_outlet)*50+1;
        if(flow_inlet < flow_outlet)
            pressure_outlet_1 += fabs(flow_inlet- flow_outlet)*50+1;
    }
}
Message("calvalue_Cmu = %f\t", calvalue_Cmu);
Message("flow_inlet = %f\t", flow_inlet);
Message("flow_outlet = %f\t", flow_outlet);
Message("pressure_inlet = %f\t", pressure_inlet_1);
Message("pressure_outlet = %f\n", pressure_outlet_1);
#endif

host_to_node_float_2(pressure_inlet_1, pressure_outlet_1);
}

DEFINE_PROFILE(INLET_PRESSURE, thread_in, index)
{
#ifdef !RP_HOST
    face_t f;
    begin_f_loop(f, thread_in)
    {
        if (PRINCIPAL_FACE_P(f,thread_in))
        {
            F_PROFILE(f, thread_in, index) = pressure_inlet_1;
        }
    }
#endif
}

```

```

    }
    end_f_loop(f, thread_in)
#endif
}

DEFINE_PROFILE(OUTLET_PRESSURE, thread_out, index)
{
#if !RP_HOST
    face_t f;
    begin_f_loop(f, thread_out)
    {
        if (PRINCIPAL_FACE_P(f, thread_out))
        {
            F_PROFILE(f, thread_out, index) = pressure_outlet_1;
        }
    }
    end_f_loop(f, thread_out)
#endif
}

```

Curriculum Vita

Da Xiao

Degrees

M.S. Mechanical Engineering, May 2019

B.S. Jilin University, Automobile Engine, June 2017